NTNU Trondheim
Norwegian University of Science and Technology
Department of Marine Technology

MASTER THESIS IN MARINE STRUCTURES

SPRING 2019

FOR

STUD. TECHN. MARTINE WILLUMSEN

Ice loading on FPSO: Stress analysis of local plate field

Work description (short description)

Exploration of resources in the Barents Sea and Arctic Ocean have increased over the past decades. The presence of sea ice is an important barrier and may cause difficulties for operations in ice-infested areas. These types of operations require structures with sufficient residual strength due to ice-induced stresses. Sea ice is a complex material and can induce high pressures when being in contact with structures. In order to understand the nature of the associated ice forces, the ice physics and ice mechanics will been studied.

For floating production, storage and offloading units located in the arctic areas forces from the ice will be acting on the hull. The dimensions of the structure are important in order to determine the consequences from the various ice interactions and will be further discussed.

Determination of ice actions is a difficult process as the magnitude of the load differs for various ice interactions. Ice actions with return periods of 100-10 000 years are extreme and may cause plastic deformations of the structure. This will be considered in more detail.

Scope of work

1. Describe different types of sea ice, their physical and mechanical properties.
2. Investigate hull-ice interactions.
3. Present and discuss different models for calculation of contact pressure acting on a floating structure due to the presence of ice.
4. Perform a review of ice classes for a floating production, storage and offloading unit located in the arctic areas provided by DNV GL, IACS and ISO 19906.
5. Establish local FEM models in ABAQUS with applied extreme loads obtained by the regulations due to ice ridges. Perform various nonlinear analyses on these models, where the importance of the stiffener dimensions will be investigated. Analyses shall be carried out through small deformations to large plastic deformations. Strain levels for the different designs shall be discussed, including the influence of mesh size.
6. Write a conclusion and recommendation for further work.

The report shall be written in English and edited as a research report including theory, description of mathematical models, description of control algorithms, simulation results,

model test results, discussion and a conclusion including a proposal for further work. Source code should be provided. It is supposed that Department of Marine Technology, NTNU, can use the results freely in its research work, unless otherwise agreed upon, by referring to the student's work.

The thesis should be submitted within 20th of June.

Professor Bernt J. Leira
Supervisor

Summary

This master thesis aims to explain how impacts of extreme ice loads affect the hull of an FPSO located in ice-infested areas. An extensive study of ice theory was conducted. Knowledge about ice physics and mechanics is important in order to better understand the forces from ice on a structure. The mode of ice failure against a structure has a significant effect on the magnitude of the ice action. Different types of ice failures may occur on the same structure depending on interaction velocity and ice condition, even during the same event.

Local models of the hull of a FPSO has been successfully designed and analysed in ABAQUS in order to find the response due to local ice actions. DNV GL, IACS and ISO 19906 provides regulations for offshore structures operating in ice-covered seas. These regulations have been used in the deign process of the models. Four different models were established with different stiffener geometry, stiffener dimensions and stiffener spacing. The response of the models were analysed using different ice pressures obtained from DNV GL, IACS and ISO 19906. The local design loads provided by DNV GL and ISO 19906 are more similar than the design load obtained from IACS. This is due to similarities in the calculation of the design load between DNV GL and ISO 19906. All three design loads resulted in stresses above the yield strength. This implies that the models will get non-linear behaviour, due to the stress-strain relationship no longer is linear. In non-linear behaviour; small changes in stresses could lead to big changes in displacement.

From the analyses with design load provided by the regulations, one could also see the importance of the stiffener dimensions. As expected, the models with tee-bar stiffeners could absorb more stresses than the flat-bar stiffeners, resulting in lower displacements of the plate. In addition, a narrower stiffener spacing also resulted in lower stresses in the plate.

The critical strains for the stiffened plates were investigated according to DNV GL's regulations. As expected, the model with tee-bars and smallest stiffener spacing had the largest critical strain. While the model with flat-bars and large stiffener spacing had the smallest critical strain. The design loads from DNV GL and ISO 19909 resulted in maximum principal strains that were less than the critical strain, while the design load from IACS resulted in maximum principal strains that were greater than the critical strains. Hence, it is important to evaluate whether or not the loads obtained from IACS might be too conservative.

Steel becomes brittle at low temperatures. Materials are in general qualified at so called "design temperatures", which typically lies 20^oC below maximum expected service temperature. In Arctic, operational service temperatures as low as -40^oC should be expected, implying that the design temperature should be -60^oC. Large deformations are expected in the Arctic as collision with icebergs is a possibility.

Sammendrag

Denne masteroppgaven forklarer hvordan ekstreme islaster påvirker skroget på en FPSO lokalisert i isbelagte områder. En omfattende studie av isteori ble utført. Kunnskap om isfysikk og ismekanikk er viktig for å bedre kunne forstå kreftene fra is på en konstruksjon. Hvordan is svikter imot en konstruksjon har en betydelig effekt på styrken av islasten.

Lokale modeller av skroget på en FPSO har blitt designet og analysert i ABAQUS for å finne responsen ved interaksjon med is. DNV GL, IACS og ISO 19906 har reguleringer for offshorekonstruksjoner som opererer i isbelagt hav. Disse reguleringene har blitt brukt i dimensjoneringsprosessen av bå de modellene og islastene. Fire forskjellige modeller ble etablert med forskjellige stivergeometri, stiverdimensjoner og stiveravstand. Modellenes respons ble analysert ved forskjellige istrykk beregnet fra DNV GL, IACS og ISO 19906. De lokale designlastene fra DNV GL og ISO 19906 er likere, sammenlignet med lastene beregnet i henhold til IACS. Dette skyldes likheter i beregningen av designlast mellom DNV GL og ISO 19906. Alle tre designlaster resulterte i en høyere spenning enn flytspenning. Dette tyder på at modellene vil oppføre seg ulineært, siden spenning-tøyingsforholdet ikke lenger er lineært. Ved ikke-lineær oppførsel vil små endringer i spenning resultere i store endringer i forskyving. Fra analysene med designlast fra reguleringene, kunne en se viktigheten av stiverdimensjoner. Som forventet kunne modellene med T-stivere absorbere mer spenning enn de med I-stivere, som resulterte i mindre forskyving av platen. I tillegg vil også en smalere stiveravstand resultere i lavere spenninger i platen.

Kritiske tøyning for de avstivede platene i modellene ble utforsket i henhold til reguleringer fra DNV GL. Som forventet hadde modellen med T-stivere og minst stiveravstand størst kritisk tøyning. Modellen med I-stivere og stor stiveravstand hadde den minste kritiske tøyning. Designlastene fra DNV GL og ISO 19909 resulterte i maksimal hovedtøyninger som var mindre enn kritisk tøyning, mens designlasten for IACS resulterte i maksimal hovedtøyning som var større enn kritisk tøyning. I dette tilfellet er det viktig å gjøre en vurdering om lasten fra IACS er litt for konservativ.

Stål blir sprøtt ved lave temperaturer. Materialer er generelt kvalifisert ved en "design temperatur", som typisk er på 20°C under maksimal operasjonstemperatur. I Arktisk kan en forvente operasjonstemperaturer så lavt som -40°C, som betyr at design temperaturen til stålet må være -60°C. Store deformasjoner er forventet i Arctic grunne muligheten for kollisjon med isberg.

Preface

This master thesis is a result of my work during the spring semester of 2019 at the department of Marine Technology under the Norwegian University of Science and technology (NTNU). The thesis is written with focus on the structural part of the marine engineering field.

I would like to express my gratitude to my supervisor, Professor Bernt J. Leira, for helpful guidance during this time.

Martine Willumsen
Trondheim, June 20, 2019

Table of Contents

List of Tables

List of Figures

Chapter 1

Introduction

Marine operations in the Barents Sea and Arctic have become more relevant over the past decades, and they are often carried out in seas covered in ice. The increase in Arctic activity is manly due to search for oil and gas, survey of ice and environment, route for transportation and lately, increased truism. These kind of operations requires structures with sufficient residual strength due to ice-induced stresses. Ice occurs in all kinds of different shapes and sizes, causing the ice to have varying strength, and hence varying load-inducing properties.

In order for operations in ice infested waters to be safe, regulation societies have developed several sets of classification requirements regarding navigation in ice. These classification requirements are possible to optimise as the knowledge gets better and experiences increases.

The calculations and estimations of ice-induced forces have proved to be difficult. It is important to notice that since ice is unpredictable, deciding an actual load pattern and resulting contact pressure on hull is difficult. Ice actions will occur throughout operations in ice, and will constantly vary in terms of force and form. Thus, it is important to ensure that structures are properly classified in order for hulls to be capable of dealing with the forces.

This master thesis is based on the project thesis written by the author, autumn 2018.

1.1 Objectives

Following topics have been examined, considering the uncertainties and difficulties connected to ice-hull interaction:

- Describe different types of sea ice, mainly focusing on their mechanical and physical properties.
- Introduction to hull-ice interactions.
- Present a review of ice classes for floating production, storage and offloading units operating in ice-infested waters, regarding model dimensions and design loads, with regulations provided by DNV GL, IACS and ISO 19906.
- An introduction to finite element method and non-linear analyses.
- A presentation of SEVAN FPU-ICE
- Establish locale finite element models in ABAQUS of the hull of the SEVAN FPU-ICE and analyse these with respect to extreme loads provided by ice ridges.

1.2 Scope and limitations

Regarding ice actions, the main focus in this master thesis have been on extreme loads. The main emphasis in the classification society has thus been on rules regarding offshore structures operating in Arctic waters.

For the FEM analyses, the main objective is to determine how the various parameters involved influence the response for the chosen local model. Thus, the focus will be on local forces. In addition, this thesis, only the first interaction between hull and ice will be investigated.

Chapter 2

Sea Ice Theory

Knowledge about ice infested areas become more and more relevant as surveys in Arctic areas are evolving. Physical and mechanical ice behaviour are important in order to understand what impacts sea ice will have on a structure. The most important features of sea ice, which affect marine operations are according to WMO (2017);

1. Its origin (weather it is sea ice or icebergs).
2. The amount of ice present (estimated according to the tenths or percentage of the sea surface covered by the ice).
3. Ice thickness (i.e. stage of development).
4. The form of the ice, whether it is fast or drift ice, and the size of the constituent floes.
5. and; movement of ice.

2.1 Physical properties of ice

In order to understand mechanical properties of ice the physical properties needs to be investigated. Most of the theory for physical properties of ice is obtained from Palmer and Croasdale (2013) and Løset and Høyland (2006).

2.1.1 Structure of ice

Water consist of two hydrogen atoms and one oxygen atom (H_2O), where the relative positions between the three of them are not fixed. Ice can have at least nine structures, and each of them is more ordered than the changing and loose structure of liquid water. The

ice form that occurs in nature at the surface of the earth is called ice Ih, the other forms are found only at much lower temperatures and higher pressure. Each oxygen atom is at the centre of a tetrahedron with four more oxygen atoms at the apices of the tetrahedron. The molecular structure of ice will consist of a hexagonal arrangement of oxygen atoms located in series of parallel planes called basal planes. Figure 2.1a illustrates the hexagonal pattern with the c-axis pointing out of plane, while figure 2.1b illustrates the horizontally arranged basal planes with a vertical c-axis. The circles represents oxygen atoms, and the lines represents hydrogen bonds.

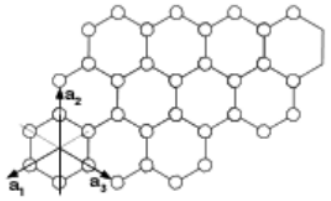

(a) Hexagonal arranged crystals with c-axis out of plane

(b) Horizontally arranged basal planes with a vertical c-axis

Figure 2.1: Ice crystals

Sea ice is a crystalline material and its properties depend on the size and orientation of its crystals, as well as its salinity, temperature, impurity and density.

2.1.2 Ice formation

Fresh water and salt water freeze in vaguely different ways. Fresh water with 0 salinity has a density maximum when the temperature is $+4°C$, and water that is either warmer or colder than this has a smaller density than the maximum. This implies that once the temperature in the top layer of the surface has reached temperature for maximum density, this water will sink and new warmer water will rise to the surface. This is an ongoing process until all the water has obtained maximum density. Further cooling will then create a less dense surface, this means that the surface layer will now transform to ice as the cooling continues even though the water below is still $+4°C$. For water with low salinity, the temperature at which the density is a maximum decreases towards $0°C$, and there is a narrowing region in which the density increases with decreasing temperature. Once the salinity reaches 24.7‰ that region disappears, and the density will always increase as the temperature falls. In sea water with a salinity greater than 24.7‰ there is no density minimum. Meaning that a cooler surface layer would always be denser than a deeper warmer layer, and so convection continues until the whole water column has cooled down. Although, at some depth there is often a density increase, called a pycnocline, and convection may cease at that level.

In addition, the presence of salt lowers the freezing point, so that ordinary sea water with salinity of 35‰ freezes at approximately $-1.8°C$. (Palmer and Croasdale (2013)).
When sea water freezes, the salt is separated from the first ice plates that form. Hence, flat plates of fresh ice form. As the ice mass continues to grow, the platelets commingle and bond one to another to form a highly saline and compliant slush called grease ice. With sustained freezing temperatures, the platelets mass thickens and grows together. Most of the sea water is displaced during this process, but between the platelets of pure ice a sea water concentrate called brine becomes trapped. The entrapment of sea water causes the ice to be salty.

The direction of the growing ice platelets, are at first randomly oriented. This applies for platelets < 0.5[mm]. But in time they become increasingly ordered, grow wider, and stack one against another. A rapid increase in grain size is associated with the competition between grains grains for growth. The transition zone is fairly thin (5 [cm] to 30 [cm]), and is the vertical portion of the ice sheet where the crystal orientation has a rapid change, see figure 2.2.

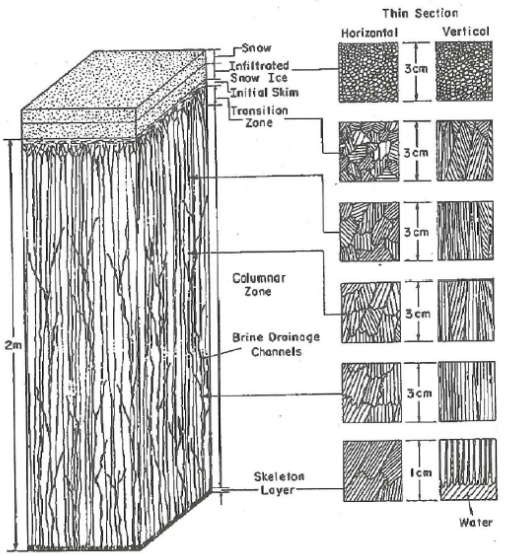

Figure 2.2: Schematic drawing sowing multiple aspects of the structure of a first-year ice. Løset and Høyland (2006)

The columnar zone is the ice below the transition zone. This ice has a rather uniform structure, where the dominant crystals have their c-axes horizontal and showing pronounced elongation parallel to the direction of heat flow. The changes of grain size with depth in the columnar zone are small, and the major portion of first-year sea sheets consist of such

columnar ice.

Brine entrapment originates in the root area of the 10 to 50 [mm] thick mushy region called the *skeleton layer* or *SK*. In this growth zone the individual ice platelets stretch into the seawater like fingers and are usually more than 10 [mm] wide and less than 0.25 [mm] thick, see figure 2.3. Each dendritic platelet freezes to its neighbour as it grows thicker at its root. A high growth rate (> 20 [mm]/day) at this stage results in platelets less than 0.5 [mm] thick, but with at low growth rate (< 5 [mm]/day), the platelets can grow to be 1.6 [mm] thick, with a related increase in crystal size. During this crystal formation process supersaturated brine that slows the rate of solidification replaces seawater at the ice growth interface.

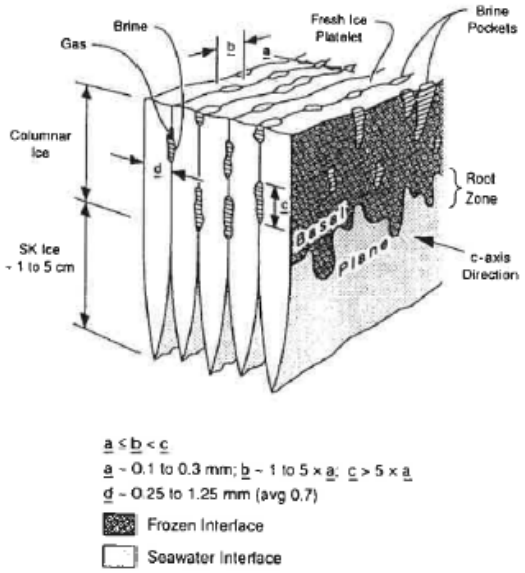

Figure 2.3: Sea ice crystal structure Løset and Høyland (2006)

Some gas and brine become trapped between the cells or platelets (figure 2.3). As the ice sheet becomes colder and continuous to grow, the film of brine between the ice platelets reduces in volume due to drainage and expulsion processes as well as freezing of freshwater from the brine to the surrounding ice surface. It is along the platelets boundaries that the salt in the sea ice is present in form of solid and liquid inclusions. The isolated brine inclusions are called brine pockets. The brine layer spacing, also referred to as the plate width, is the most important parameter in characterising the substructure. Brine drainage and expulsion occur along a flow route that resembles the branches and trunk of a tree, called drainage channels and tube, respectively.

2.1.3 Density and porosity in ice

Density is a measure of mass per unit of volume and describes the compactness of a material. The strength of sea ice is related with the density, and the density depends on the the porosity. Ice consist of pure ice, trapped gasses, salts and brine pockets. The total porosity is a sum of gas and brine fractions. The relative volume of brine existing in sea ice will affect thermal, electrical and mechanical properties of ice. In addition, the volume of gas and air in the ice pose a major portion of the total portion of the total porosity. Hence, knowledge about the total porosity is important. Referring to Cox and Weeks (1983) in this section and Løset and Høyland (2006). The density could be computed by equation 2.1.

$$\rho_i = (1 - \eta_a)(1 + \frac{S_i}{\alpha T_i \rho_w}(\rho_w - \rho_{pi}))\rho_{pi} \tag{2.1}$$

Where ρ_i is the density of sea ice, η_a is the volume of air in the unit volume of sea ice, S_i is the salinity of ice, α is a constant normally equal to $-0.0182[\frac{1}{^\circ C}]$. T_i is the temperature in ice, ρ_w is the density of water and ρ_{pi} is the density of pure ice.

2.2 Mechanical properties of ice

The remaining theory in this chapter is withdrawn from Løset and Høyland (2006). The ice strength depends on several factors, and it is difficult to describe the exact impact from the individual parameters. Interaction between the various parameters will hence impact the ice strength. Dominating parameters regarding ice strength is; porosity, grain size, temperature and load rate. Ice is a crystalline material equal to metals, and have both brittle and ductile behaviour. There are two factors which distinguish ice from metals and increases the material behaviour complexity; the grains in ice are relatively large and, ice exists only close to its freezing point.

Sea ice is a multi-phase material consisting of pure ice, solid salts and brine- and air pockets. Hence, sea ice is a complicated material to study. Material behaviour consists of two parts; fluid and solid material behaviour. Hence, both linear and non-linear material behaviour need to be included to describe the solid part, and visco-elastic and visco-plastic behaviour to describe the fluid part. Fluid behaviour is time dependent and will be negligible due to the short impact time during ship-ice interaction.

2.2.1 Elastic modulus

In the time-independent one-dimensional case, the stress-strain relation is expressed using Hooke's law. The elastic modulus can then be expressed as:

$$E = \frac{\sigma}{\epsilon} \tag{2.2}$$

Where σ is the applied stress given by an applied force, F over a nominal area, A_{nom}. ϵ is the total strain. For short-term loading due to short impact duration, the most important behaviour is considered elastic-plastic. The ice will accordingly undergo three different phases; elastic deformation prior to first yield, plastic strain hardening prior to the peak stress and lastly, softening after reaching the peak stress, illustrated in figure 2.4.

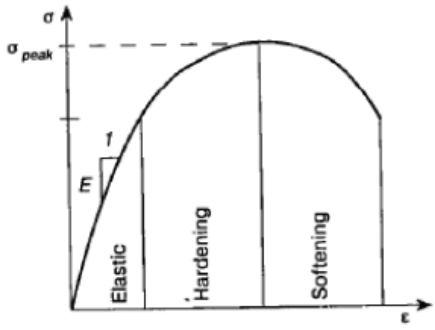

Figure 2.4: Stress-strain diagram for a linear-elastic-perfect plastic model, Løset and Høyland (2006)

The elastic strain of ice is a result of deformation of atomic bonds, and it is a reversible process. There are several papers that provide different relationships between Young's modulus and key parameters such as temperature and porosity.

2.2.2 Failure models of ice

Two simple models to describe the failure strength or stress are Tresca and von-Mises models where only one material property is needed to describe the failure stress or strength. The Tresca criterion says that the material behaves elastically as long as the shear stress, τ, is below a certain material capacity, R_s;

$$\tau \leqslant R_s \tag{2.3}$$

It is assumed that the material fails on the plane where the maximum shear stress acts, that is $\pm 45°$ to the principal stresses (σ_1, σ_3). It further implies the same strength in compression as in tension. This model fits well to a wide range of engineering applications, especially for metal that exist far away from their melting temperature. However, many geophysical material such as ice, rocks and soil are weaker in tension and pressure dependent behaviour must be accounted for. The simplest model to account for this phenomena is the Coulomb-

Mohr model where a critical combination of the shear- and normal stress on a plane results in failure as given by equation 2.4:

$$\tau \leqslant c + \sigma \cdot tan\phi \tag{2.4}$$

In figure 2.5 σ and τ are the normal stress and shear stress respectively in a given plane, C is the cohesion and ϕ is the angle of internal friction. If ϕ equals ±45°, the Tresca criterion applies.

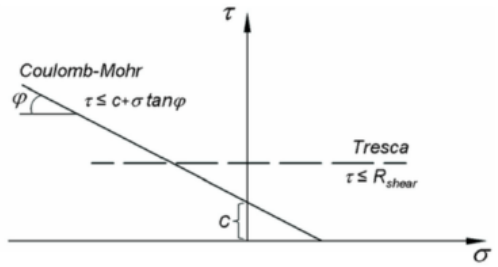

Figure 2.5: The Tresca and Coulomb-Mohr models in the $\tau - \sigma$ plane Løset and Høyland (2006)

The tensile capacity for ice is even less than given by the standard Coulomb-Mohr criterion and a tensile cut-off may be introduced. Figure 2.6 illustrates that the failure takes place on the plane where a critical combination of normal and shear stresses exists.

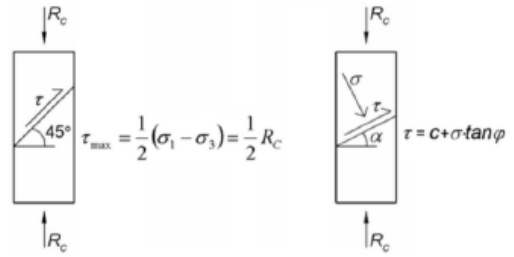

Figure 2.6: The failure planes in uniaxial compression tests, Løset and Høyland (2006)

2.2.3 Material properties and parameters

There are several parameters that affect the mechanical behaviour of materials, and usually one distinguishes between *State variables* and *Type of material*. State variables are such parameters as the temperature, the strain, the stress, the loading rate etc. For ice the temperature and the loading rate ($\dot{\sigma} or \dot{\epsilon}$) are the two most significant ones. The type of ice is basically defined by the grain orientation and size, as well as the shape and size of the pores.

Ice becomes in general weaker and softer with increasing temperature, grain size and porosity. Temperature has two important effects on ice; it affects the porosity and, the temperature itself affects the mechanical behaviour. The effect of the loading rate is schematically explained in figure 2.7a. The strength increases with increasing strain-rate until brittle failure take over, then the strength decreases. This is due to the development of cracks.

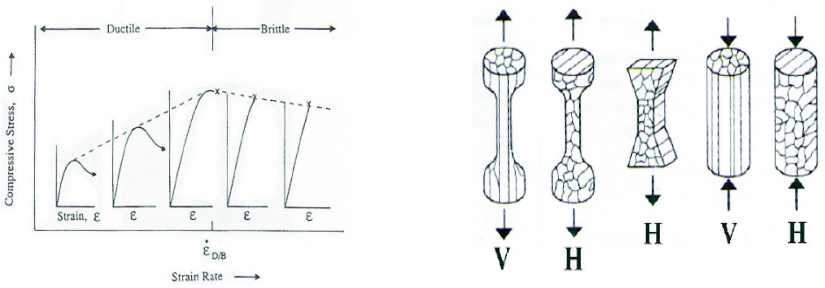

(a) One-dimensional ice strength and behaviour as a function of strain rate **(b)** Uniaxial tensile and compression experiments on ice with different orientation

Figure 2.7: Løset and Høyland (2006)

Figure 2.7b shows different grain direction and the according behaviour relative to tension and compression. The load direction relative to the grain direction is hence also a very important parameter. Since ice grows in a vertical direction the columns of grains will be vertical. Ice will have relatively greater strength in vertical compression (along the c-axis) compared to horizontal compression (along the basal planes). This is due to slipping along the grains, and this occurs more easily than breakage between the basal planes. Empirical formulas have been derived for compression strength of ice relative to the grain boundaries.

2.2.4 Failure modes of ice against a structure

The mode of ice failure against a structure is a very important parameter because the maximal pressure that ice may endure determines the maximal ice action on the structure and this pressure, in turn, depends on the ice failure mode. Various types of failure (compressive, yielding, flexure, tensile, etc.) take place depending on the strength level, stress distribution, ice velocity, and the structures shape. For example, as the ice resistance to compression is significantly higher than for bending, the conditions, which induce the ice failure by flexure, will correspond to lower actions. Different modes of ice failure may even exist for the same structure (for example vertical). They depend on the velocity, the ice thickness and feature size, a rubble pile up near the structure, etc. The modes may replace each other during the same event depending on the instant local condition of

interaction. Nevertheless the interaction events could be made more understandable with approximate classification of the failure modes. Figure A.19 illustrates the different failure modes of ice observed in laboratory experiments and in full scale, conducted by Blanchet and Badra-Blanchet (1989).

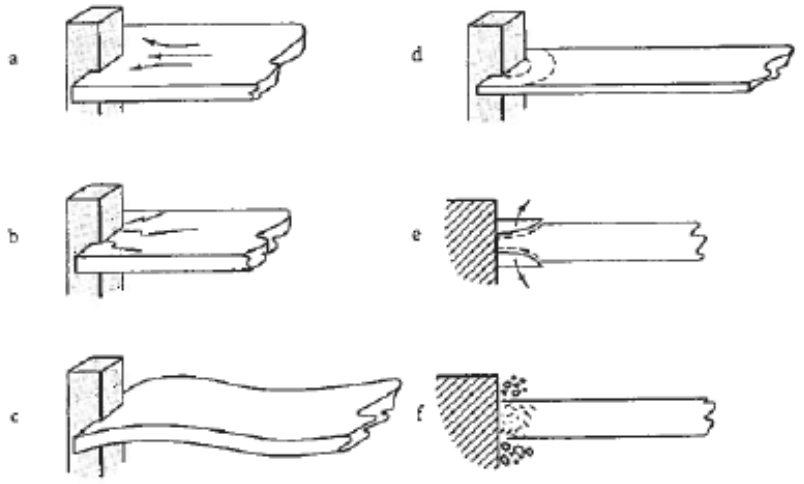

Figure 2.8: Principle failure mechanisms observed during laboratory indentation experiments: (a) creep, (b) radial cracking, (c) buckling, (d) circumferential cracking, (e) spalling, (f) crushing (Løset and Høyland (2006))

The following description of failure modes was offered:

a) ***Creep*** develops at very low indentation rates, at speeds below 1-3 mm/s, when the ice yields. No cracks form in the ice and the deformation develops continuously. The contact between the structure and the ice is perfect and the ice covers the whole front side of the structure near the waterline. Therefore, actions during the creep are often close to maximal. Creep is most relevant for narrow structures.

b) ***Radial cracks*** are associated with tensile failure. The develop above specific stress levels and especially at high aspect ratios. If the structure is rectangular, the radial cracks develop from the structures' corners. The crack can also form in front of a structure with a cylindrical cross-section.

c) ***Buckling*** is especially characteristic for wide structures and thin ice. This type off failure is usually connected with radial or circumferential crack formation.

d) ***Circumferential cracks*** may form as a result of elastic buckling, or because of an out-of-plane bending moment caused by the eccentric action conditions (for instance on slopes).

e) ***Spalling***-formation of out-of-plane horizontal cracks which grow away from the contact zone and divide the ice into layers. Their length depends on the ice sheet velocity, where higher velocity results in smaller length. Formation of ice fragments at the top and bottom of the of the ice sheet is the final stage of the spalling effect.

f) ***Crushing*** happens at high rates, ice crushes continually in a brittle manner against both wide and narrow structures, resulting in a non-simultaneous partial contact and non-uniform pressure ovre the nominal contact area. The crushing process often controls the design action.

g) ***Bending*** is in most situations linked with ice interacting with sloped structures. Usually circumferential and radial cracking develops due to the ice sheet riding up or down the slope. The predominant type pf these cracks depends on the ice thickness and the width of the structure.

g) ***Alternating creep and brittle failure*** arises at intermediate speeds. The interaction between an advancing ice sheet and structural deformation produces alternating creep and brittle crushing in the same event, resulting in saw tooth form of action. During each cycle of intermittent crushing, the ice sheet deflects the structure while undergoing creep deformation with increasing deformation. The stored energy in the structure is released to move the structure back to its original position when the ice sheet fails at a certain loading level. This results in high relative speed with respect to the ice and thus causing brittle failure.

2.3 Classification of sea ice

Several forms of floating ice may be encountered at sea, but the most common is the sea ice, which is the result from the freezing of the sea surface. The other forms are river ice and ice of land origin. Rives ice is detected in harbours and estuaries where it is kept in motion by tidal streams. River ice normally presents only a temporary hindrance to shipping. Ice of land origin is mainly icebergs, which are large masses of floating ice derived from glaciers. The underwater draught and mass of a berg, compared with its height and mass above water varies a lot with different shapes and composition of bergs. The underwater mass of a Greenland glacier derived from a floating ice shelf is usually larger than the underwater mass of icebergs derived from Antarctic iceberg. Both sea ice and icebergs can be dangerous to shipping and will always have an effect on navigation. The theory of classification of ice is mostly obtained from WMO (2006).

2.3.1 Ice less than 30 centimeters thick

The first indication of ice appearance is small ice spicules or plates in the top few centimeters, known as frazil ice. As cooling continuous the frazil coalesces to form grease ice. Further, a layer of slush may be formed under near freezing, but yet ice-free conditions, with snow falling on the surface. These forms may be regrouped to form shuga by the action of wind and waves, and they are all classified as new ice.

With further cooling, and with potential snow falling on the surface, sheets of ice rind are formed. The ice growth depends on the rate of cooling, the salinity of the water and the wind. Ice rind is formed when water with low salinity freezes into a thin layer of brittle ice that is almost salt free. Ice rinds may be up to five centimeters thick. When water with high salinity freezes, and if the process in addition is rapid and the wind very light, the ice will get an elastic property which is characteristic of nilas. Nilas is subdivided into dark and light nilas, according to its thickness which is within the range 5-10 centimeters. Ice rind, dark and light nilas is referred to as nilas ice.

Pancake ice is formed in the boundary between two water layers of different salinity, the lower layer with high salinity has a temperature below the freezing point of the upper layer of lower salinity. The pancakes will eventually surface due to buoyancy forces. Pancakes, nilas and ice rinds may thicken into grey-white- and grey ice, the first attaining thicknesses up to 30 cm thick and the other being 10-15 cm thick. These forms of ice are collectively referred to as young ice, which may break into ice cakes, pancakes or floes of varying size due to rough weather.

2.3.2 Ice with thickness range from 30 cm - 2m

The next level of development is first-year ice (FY) and is subdivided into thin, medium and thick categories. The thin FY has a thickness of 30-70 cm, the medium FY has a range of thickness from 70-120 cm while in polar areas thick FY may attain a thickness of approximately 2 meters by the end of the winter.

2.3.3 Old ice

Thick first year ice may survive the summer season and is then classified as old ice (MY). This category is further subdivided into second year and multi year ice depending on whether the floes have survived one or several summers. The thickness of old ice is usually in the range of 120-500 cm or more prior to the onset of the melt season. Old ice can generally be recognised by a bluish surface colour which are in contrast to the greenish tinge of first year ice.

2.3.4 Classification of sea ice by age - summary

Sea ice	Description
New ice	Newly formed ice, where the ice crystals are only weakly frozen together
Nilas	Thin and elastic ice that is easily bent under pressure. May be up to 10 cm thick
Young ice	Transition between nilas and first year ice. The thickens in the range 10-30 cm.
First year ice	Ice with one winter of growth, thickness up to 2 meters.
Old ice	Ice that has survived one or multiple summers. Thickness range 1.2-5 meters.

Table 2.1: Types of sea ice

2.3.5 Location of sea ice

Sea ice will behave differently regarding its position in relation to land and open ocean. The position of the ice will decide what kind of boundary conditions the ice is exposed to, thus determine ice behaviour. Løset and Høyland (2006) defines the following classes of ice locations seen in table 2.2.

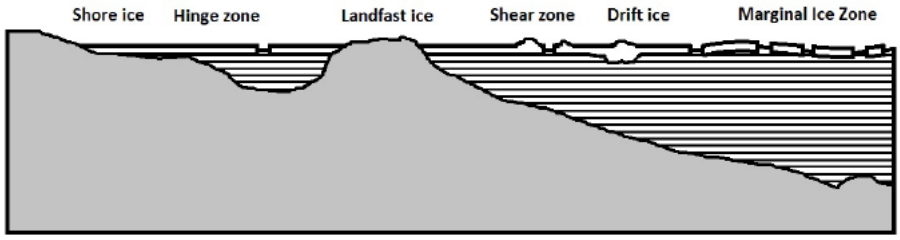

Figure 2.9: Ice classification by location (Løset and Høyland (2006))

Ice class	Description
Shore ice	Fixed to the shore line and forms the transition to the landfast ice, impacted by the shore.
Landfast ice	Horizontally fixed to the shore line and is hence only able to move vertically with tide water.
Shear zone ice	The transition from landfast ice to drift ice, characterized by large deformations.
Drift ice	Free to move and is defined by the ice concentration factor C_i. Will have different motion regrading the level of ice concentration.
Marginal ice zone (MIZ)	Transition from drift ice to open ice.

Table 2.2: Classification by location

The ice concentration factor is defined as

$$C_i = \frac{A_{Ice}}{A_{Ocean}} \tag{2.5}$$

Where A_{Ice} is the total area of ice that exists in a certain area A_{Ocean}. Figure 2.10 illustrates the difference between the areas that defines the concentration factor.

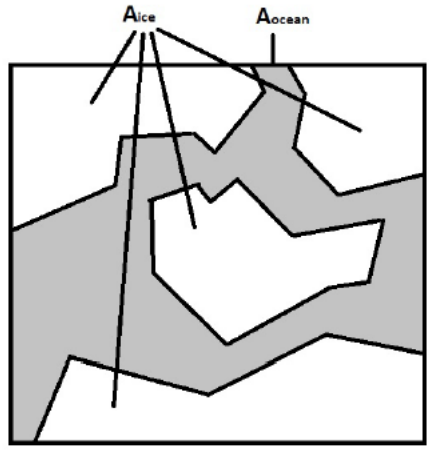

Figure 2.10: Areas defining the ice concentration factor

2.3.6 Classification by feature type

Sea ice is also divided into different groups regrading the degree of deformation. Various feature types of ice have different size, thermo-mechanical- and mechanical properties. WMO (2006) differs between two categories of feature types; undeformed ice and deformed ice. Undeformed ice has little to no mechanical deformation, while deformed ice have mechanical deformation, typically deformed by the surrounding environment such as winds, currents and Coriolis forces. The undeformed ice is usually called level ice which means that that it only consist of one layer of ice. Deformed ice is often subdivided into three groups; rafted ice, broken ice and ice ridges. The broken ice is often located in the marginal zone where waves break the ice into smaller bits. Rafted ice and ice ridges are further explained in detail.

Ice surface becomes deformed where it is being exposed to pressure. This may result in rafting of new and young ice. Rafting is when one ice floe overrides its neighbour, see figure 2.11. A driving force F_R must exceed the load capacity F_0 of an ice sheet. The driving force must then be able to compress the sheets sufficiently for overriding to occur. This is an ongoing process until the friction forces, τ_{ii}, are greater than the driving force.

This process may be repeated several times in the same area, implying that the ice could obtain more than double the thickness as multiple layers override each other.

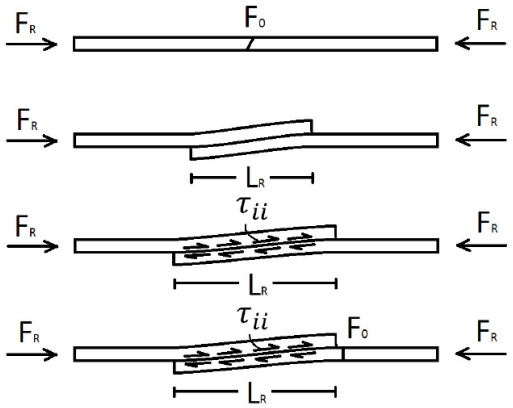

Figure 2.11: Illustration of rafting, Stephan (2017)

In thicker ice rafting leads to the formation of hummocks and ridges according to the pattern of the convergent force causing the pressure, see figure 2.12. During this process of ridging and hummocking, pieces of ice are piled up above the general ice level and large quantities of ice are suppressed downward to support the weight of the ice in the ridge or hummock. The process requires a driving force, F_R, greater than the capacity of loading, F_0, to break the ice into smaller pieces. This process continuous until $F_R < F_0$ as the capacity then is greater than the current and wind forcing the ice together. The draught of an ridge can be three to five times greater as its height and these deformations are thus major impediments to navigation. Newly-formed ridges are usually less difficult to navigate through than older, weathered and consolidated ridges.

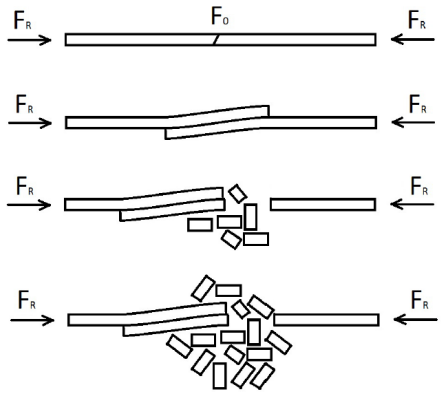

Figure 2.12: Illustration of ridging, Stephan (2017)

Sea ice ridges are complex objects with a wide variability of shapes and sizes, this has hence made their characterisation difficult. Some general information on ridge properties has emerged from numerous studies that have been made to measure the properties of ridges. Ridges have been categorised by their mode of formation (either shear or compression), but this method is not unambiguous, since it is not always clear how the ridge was formed. A more common method is to categorise the ridge based on its age - either first-year or multi-year ridge (Timco and Burden (1996)). When first formed, a ridge is simply a pile of unconsolidated rubble (broken ice), and it will eventually become to some extent consolidated by refreezing, in particular below the water line. Pressure ridges usually have surface sails above sea level and underwater keels below the water line. Sea ice ridges can be extremely large and can generate high loads during interaction with offshore structures, hence the characteristics of sea ice ridges are important.

The structure and cross section of a ridge varies greatly and the shape of a ridge is highly dependent on its age. Newly formed first-year ridges consists of poorly bonded individual ice pieces, figure 2.13 shows a schematic illustration of a first-year ridge. As winter progresses, the core of the ridge consolidates as water between the ice rocks freezes. Multi-year ice ridges have survived a number of melt seasons. The melt water emerged during the summer months will drain down into the ridge core and refreeze during the winter, creating a solid mass of ice (Sand (2008)).

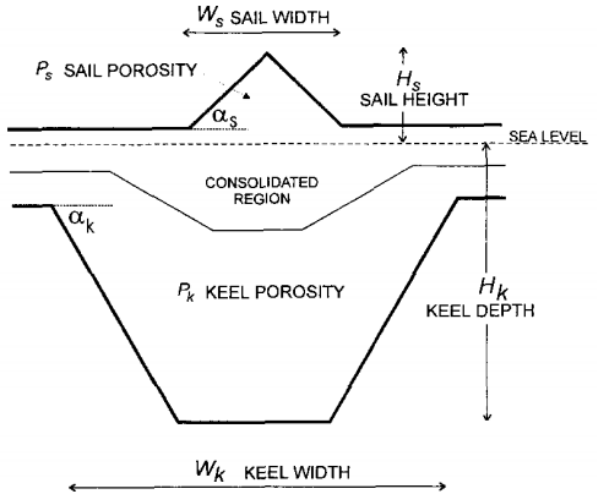

Figure 2.13: Illustration of of a first-year ridge showing the definition of terms, Timco and Burden (1996)

2.3.7 Movement of sea ice

Sea ice is divided into two main types according to its mobility. One type is drift ice, which is continuously in motion under the impact of wind and current stresses. The other type is fast ice, which is attached to the coast or islands, and does not move.

Wind causes the drift ice to move approximately in a downwind direction. The rate of movement due to wind drift depends not only on the wind speed, but also on the concentration of the drift ice and the extent of deformation (see above). There is much more freedom to respond to the wind in open ice compared to packed ice or consolidated ice, where space is very limited. There is no visible water within the compacted ice or consolidated ice where the floes are frozen together. A reasonable average rate of ice drift caused by the wind in closed ice is two percent of the wind speed, but this rate may be much higher for ice drift encountered in open sea.

A force is exerted on drift ice by currents that are present in the upper layer of the water. currents are generated from for example the tidal. It is generally very difficult to differentiate between current- and wind induced ice drift, but in any case where both are present the resultant motion is always the vector sum of the two. The average long-term transport is dominated by the prevailing surface current, whereas the short-term movements are normally predominated by wind stress.

Chapter 3

Ice interaction with structure

The mode of ice failure against a structure has a significant effect on the magnitude of the ice action. Different types of ice failures may occur on the same structure depending on interaction velocity and ice condition, even during the same event.

3.1 Vertical- and Sloped Structures

The structure geometry is an important factor in determining ice actions. Key design features include vertical- or sloping waterline geometry (see figure A.19), the structure type (multi-leg, caisson or monopod), the plan shape of the structure and the plan dimensions. Vertical- and sloping waterline geometry will be further discussed in this section.

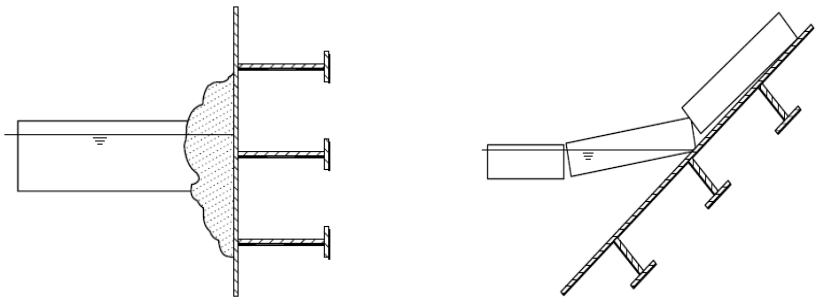

(a) Crushing failure, vertical structure **(b)** Bending failure, sloping structure

Figure 3.1: Failure modes ISO 19906:2010 (2014)

The structures profile is a key issue. Structures with vertical walls in the waterline region generally experience greater ice actions than sloping structures for similar waterline

dimensions. Ice actions are usually less for sloping structures, except in situations where large amounts of ice rubble accumulate on the sloping surface. If this situation occur, flexural failure can be impeded and mixed modes or different modes of failure can occur with potentially larger actions.

The plan shape of a structure is less important, except in situations where a corner of a rectangular structure is oriented towards the desired ice motion direction. Generally, the waterplane form of a structure has a $10 - 15\%$ influence on the magnitude of global ice actions. The plan dimensions of a structure influence the magnitude of ice actions. Many observations and experiments demonstrate the existence of a size effect, whereby the global or effective pressure (which is the total action divided by the nominal contact area) for a narrow structure is higher than for a wide one.

The ice can fail in different modes when a sheet of rafted ice or level ice acts on a vertical structure. These includes flexural failure modes such as buckling and bending, vertical (radial) splitting and crushing. Crushing is usually the dominating ice actions for vertical structure scenarios. If the structure has a sloping face, the ice often fails in flexure as it often rides down or up the face. In shallow water, rubble accumulations on the face of the structure may alter the mode of failure from crushing or flexure to a rubbling or mixed mode failure. Large rubble accumulations interacting with the seabed may buffer the ice actions and eventually prevent the transfer of actions to the structure.

Vertical structures

Crushing refers to a complex compressive failure process, that involves the development of a damaged layer as well as sequential development of spalls or flakes, and horizontal splits or cleavage cracks. Observation on ice-structure events at full scale and medium scale have shown that response of ice to higher rates in these interactions is profoundly irregular. Medium scale field tests, with interaction areas on the order of a square meter, have shown that damage processes such as creep occur at very low velocity ($\leq$ 1 mm/s). At higher velocity rates, spalls and fractures occur, resulting in high pressure zones (hpz's) in the contact area between the ice and the structure. High velocity rates also cause fracturing of large pieces of ice resulting in areas of little or no pressure. The result is that some narrow line-like areas or small patches are subjected to high pressures and others to little or no pressure. These hpz's have an important effect on local ice actions given in ISO 19906:2010 (2014).

Sloped structures

Offshore structures with a sloping surface may be considered as an alternative to a vertical structure. Level ice that interacts with a sloping structure is more likely to fail in a flexural failure mode. Ice actions in flexural failure modes can be significantly lower than in a

crushing failure mode. Sloping ice-breaking surfaces can also reduce ice actions from ice ridges. There exists multiple types of sloping structures, but for a offshore structure a conical shape is often the preferred shape due to its symmetrical plan shape.

sloping structures break the oncoming sheet ice by deflecting it either downwards or upwards. The resulting ice action has both a horizontal and a vertical component. The horizontal and vertical components of ice action on a downward breaking structure are less relative to those acting on an upward breaking structure of the same slope angle and size. In a downward breaking structure, the vertical component of the ice action is directed upwards, this reduces the effective shear resistance at the structure-seabed interface. Ice interaction with a sloping structure is a complicated process that involves failure of intact ice, ride-up of broken ice, accumulation of ice rubble on the slope, and subsequent clearing of the rubble accumulation.

Ice rubble may also accumulate under the ice sheet, further complicating the interaction process. This implies that the maximum ice action acting on a sloping structure is a function of several different parameters including bending, compressive and shear strengths of the ice sheets, density of ice, friction coefficient between ice and structure surface, presence of snow, and finally the height and geometry of the ice rubble. Figure 3.2 depicts level ice action components for a two-dimensional interaction with a downward breaking structure.

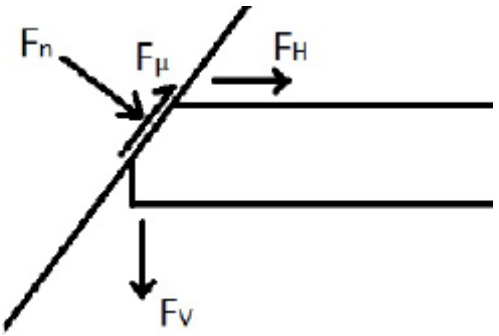

Figure 3.2: Two-dimensional ice action components on a sloping structure

The vertical and horizontal component of ice action expressed by the normal force are as given by equation 3.1:

$$\begin{aligned} F_V &= F_n(sin(\alpha) - \mu cos(\alpha)) \qquad [N] \\ F_H &= F_n(cos(\alpha) + \mu sin(\alpha)) \qquad [N] \end{aligned} \tag{3.1}$$

Where F_n is the component normal to the structure surface, α is the inclination angle of

the structure surface from the horizontal, expressed in radians, and μ is the coefficient of kinetic friction between the ice ans the structure surface.

The relationship between the vertical and horizontal components is given by:

$$F_V = \frac{F_H}{\zeta}$$
$$Where \quad \zeta = \frac{cos(\alpha) + \mu sin(\alpha)}{sin(\alpha) - \mu cos(\alpha)} \tag{3.2}$$

As long as the input data and assumptions are appropriate, theoretical models developed to compute level ice actions on sloping structures can provide reasonably accurate estimates of ice action.

3.2 Floating structures and ice management

Ice forces on a moored floating platform system are generally more complex than on a fixed platform, but the same principles of ice mechanics apply. When designing a floating system, the mooring line loads are also required, in addition to the global load applied from the ice to the vessel. These are not necessarily the same due to the inertia forces and the compliance of the system. If the ice engineer can supply the ice loading ramp describing the built up ice loads with relative distance moved by the ice, then the marine engineer may calculate the response of the system and accordingly the mooring loads.

In reality, floating structures will not be designed for interaction of the worst ice features in a region due to mooring lines have limited load capacity according to Palmer and Croasdale (2013). It is common to employ ice management (either towing or breaking an ice feature), and also the the ultimate procedure of disconnection, in order to avoid overloading the vessel itself and the mooring lines. Ice management is a complex combination of detection, monitoring, ice breaking and ice towing within the context of alert zones that require certain procedures to safeguard the well and the crew, with increasing hazard level.

It is necessary to consider global ice action for the stationkeeping system and hull for the parameter distributions associated with managed ice when the floating structure is connected. Those features at the upper end of the managed ice distribution for which the ice actions approach the capacity of the stationkeeping system are of particular concern. In addition, it is necessary to consider ice actions on the hull when in transit and for disconnected states.

Managed ice loads are generally lower than unmanaged ice loads, and interaction with icebergs are in theory also avoided. However, it is of interest to know the magnitude of loads from unmanaged ice as it represents an upper limit of loads, as ice management may fail, resulting in larger loads on the floating structure.

3.3 Local ice loads

The design of offshore structures in arctic water depends on both local and global ice loads. The ice loads are contact forces that are transmitted to the structure by interaction with ice, floes, ice ridges or icebergs. Local ice actions on offshore structures in ice-infested waters have been researched on the basis of relevant theoretical and full-scale methods for decades. Local ice actions apply for different contact areas which contribute to the overall capacity to withstand ice pressure. ISO 19906 provides regulations for local scantlings of structural configurations as plate thickness, frame spacing and stiffeners to fulfil the most critical cases that a conical structure may encounter in ice-infested waters, and will hence be further discussed along with regulations provided by DNV GL and IACS in the upcoming chapter.

Chapter 4

Classification societies

All offshore structures need to be classified according to rules from a classification society in order to operate commercially. Offshore structures in ice-infested areas are exposed to loads they would not experience in other regions, and for this particular reason specific classification rules have been developed. Several parameters should be considered in the design phase for a offshore structure operating in ice. Particularly environmental parameters and operational limits are important when deciding the class type. It exist multiple classification societies for offshore structures operating in arctic regions. Classification requirements provided by DNV GL and IACS will be further discussed in this chapter with regards to local dimensions and local ice pressure. In addition ISO 19906 will be briefly mentioned.

4.1 DNV GL

DNV GL's rules for Classification of Floating Production, Storage and Loading Units refers to DNVGL (2013), Ships For Navigation in Ice, regarding ice loading and structural requirements for a FPSO operating in ice-infested areas.

4.1.1 Ice classes

DNV GL provides several classes for ice going vessels, depending on the area of operation and the degree of exposure to ice. The classes are normally divided into duration of operation in ice infested waters and impact conditions, regarding feature type, interactions and age. For vessels intended for service in waters with light ice conditions apply class notation *ICE-C* or *ICE-E*. For vessels intended for Arctic and ice breaking service apply class notation *ICE-05* (or *-10* or *-15*) or *POLAR-10* (or *-20* or *-30*), whichever is relevant.

Northern Baltic Area

Requirements to vessels for service in the northern Baltic during winter, or areas with similar conditions. These notations are presented in table 4.1. DNV GL provides four different ice class notations which are equivalent with the *Finnish-Swedish* ice classes for the northern Baltic. An ice strengthen ship is assumed to operate in open sea conditions corresponding to a level ice thickness not exceeding the ice thickness, h_0.

Ice class notation	h_0
ICE-1A*	1.0
ICE-1A	0.8
ICE-1B	0.6
ICE-1C	0.4

Table 4.1: Ice condition for northern Baltic ice classes

Vessels in *ICE-1A** are normally capable of navigating in difficult ice conditions without the assistance of icebreakers. Vessels in *ICE-1A* are capable of navigating in difficult ice conditions, with the assistance of icebreakers when necessary. Vessels in *ICE-1B* and *ICE-1C* are capable of navigating in moderate and light ice conditions respectively, with the assistance of icebreakers when necessary.

4.1.2 Classification for Polar areas

Requirements for icebreakers, passenger- and cargo vessels operating unassisted in ice-infested waters of sub-Arctic, Arctic and/or Antarctic regions. Each class is designed for a particular condition of ice, regarding strength of the ice cover and thickness. The *ICE-XX* classes are designed for winter ice with pressure ridges, and they are limited to no ramming. The *POLAR-XX* classes are designed for winter ice with pressure ridges, multi-year ice-floes and glacial ice inclusions, and they are limited to endure occasional ramming. The *XX* notation correspond the expected average ice thickness. The *Icebreaker* class is designed for the same type of ice encountered as the *POLAR* classes, the difference is that the *Icebreaker* class can take several attempts of ramming to break the ice. The different assigned ice properties are presented in table 4.2. For the Sevan FPU-ICE, which has the intention of operating in the Arctic for an extensive time period, the class notation POLAR-30 is a suitable class.

Class notation	Nominal ice strength σ_{ice} [N/mm^2]	Nominal ice thickness (h_{ice} [m]
ICE-05	4.2	0.5
ICE-10	5.6	1.0
ICE-15	7.0	1.5
POLAR-10	7.0	1.0
POLAR-20	8.5	2.0
POLAR-30	10.0	3.0
Icebreaker	As above	As above

Table 4.2: Ice conditions for polar ice classes

4.1.3 Local ice pressure for polar classes

In this thesis local loads applied on the model will be further discussed. However, it is important to keep in mind that there exist several other important loads that the offshore structure is exposed to in ice infested waters.

All polar going vessels should withstand local ice pressure as it is defined for the different ice class notations, and as applied to the different ice reinforced areas. The design pressure shall be applied over a corresponding contact area reflecting the type of load in question. The local design ice pressure is defined in equation

$$p = F_B \cdot p_0 \qquad [kPa] \tag{4.1}$$

F_B is a correction factor for the design contact area, and is defined as:

$$\begin{aligned} F_B &= \frac{0.58}{(A_C)^{0.5}} \qquad for \quad A_c \leq 1.0m^2 \\ &= \frac{0.58}{(A_C)^{0.15}} \qquad for \quad A_c > 1.0m^2 \end{aligned} \tag{4.2}$$

Where $A_c = h \cdot w$, as illustrated in figure 4.1. h is the effective height of the contact area, generally equal to $0.8h_{ice}$ in the stem area. w is the critical width of the contact area.

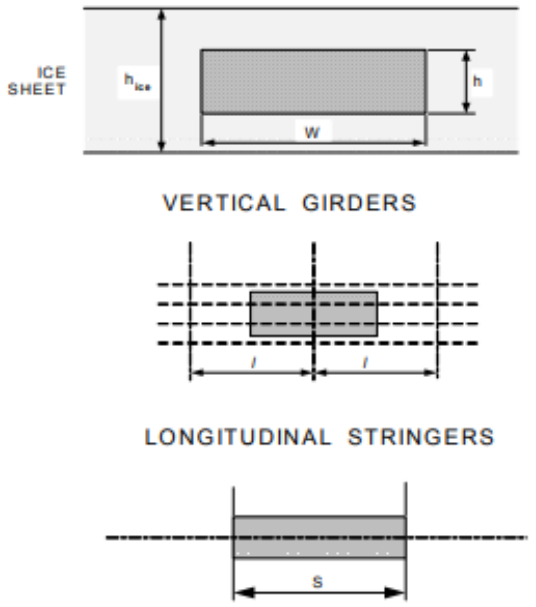

Figure 4.1: Design contact area provided by DNVGL (2013), applied for local ice pressures

The basic local ice pressure is defined in equation 4.3

$$p_0 = 1000\, F_A\, \sigma_{ice} \qquad [kN/m^2] \tag{4.3}$$

Where F_A is the correction factor for ice reinforced area in question, which in general is 1.0 for the stern area in ships with class notation Icebreaker or Polar. σ_{ice} is the nominal ice strength, which is $10[N/m^2]$ for POLAR-30.

Figure 4.2 shows the relationship between stiffener spacing and local design pressure for class notation POLAR-30, for $A_C \geq 1.0m^2$. The pressure increases as the stiffener spacing decreases. Concerning the local hull design; plate thickness, stiffener spacing and steel quality are important parameters in optimising the design regarding costs, weight and safety.

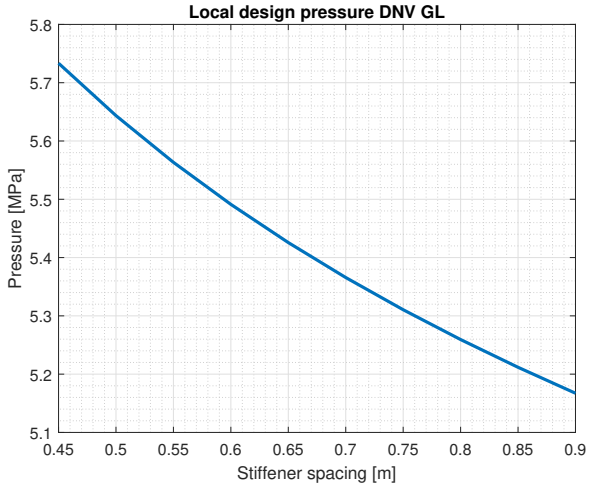

Figure 4.2: Local design pressure depending on the stiffener spacing for POLAR-30

4.1.4 Local plate dimensions

Plate thickness

The thickness of the plate exposed to patch load is defined as:

$$t = 23\, k_a\, \frac{s^{0.75}}{h_o^{0.25}} \sqrt{\frac{k_w p_0}{m_p \sigma_f}} + t_k \qquad [mm] \tag{4.4}$$

k_a is the aspect ratio factor for plate field, and is in the range of 0.85-1.0 depending on the ratio between stiffener spacing and length. s is the stiffener spacing in meters. h_o is equal to the effective height of contact area, which for POLAR-30 is 1.2 [m]. k_w is the influence factor for narrow strip of load, perpendicular to s, with a maximum value of 1. m_p is a bending moment factor as a function of ice thickness and stiffener spacing. σ_f is the yield stress of the steel, and t_k is a corrosion addition.

Stiffener dimensions

The stiffeners are aligned transverse to the water line. The section modulus shall not be less than:

$$Z = \frac{520 l^2 s^{1-\alpha} p_0 w_k}{m_e 0.9 \sigma_f h_0^{\alpha} sin(\beta)} \qquad [cm^3] \tag{4.5}$$

l defines the span of the transverse stiffeners. α depends on the contact area A_c, and is in this case equal to 0.5. w_k is the section modulus corrosion factor, m_e is the bending

moment factor and is equal to 12.9. β equals the angle of the web with shell plating defined as:

$$\beta = arctan\frac{tan(\gamma)}{sin(\theta)} \tag{4.6}$$

γ and θ are defined in figure 4.3

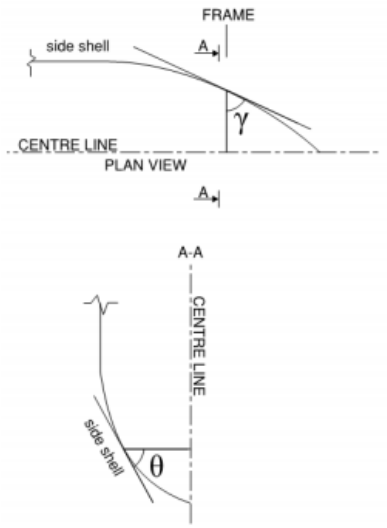

Figure 4.3: Determination of β-angle

4.2 IACS

4.2.1 Review of ice classes

A brief review of the ice classes provided by IACS will be presented in this section, and all the information is obtained from IACS (2016). IACS defines the polar classes into seven different classes, where the ice conditions are defined by WMO Sea Ice Nomenclature. The classes intend to divide vessels into different operational capabilities and strengths. Table 4.3 presents the classes and ice description regarding operational limits. The class that is most similar to DNV GL's POLAR-30 is PC 1, and will hence be further assessed considering local design loads and contact area. In addition, a short review regarding plate and stiffener requirements will also be presented.

Class	Ice description (based on WMO Sea Ice Nomenclature)
PC 1	Year-round operation in all polar waters
PC 2	Year-round operation in moderate multi-year ice condition
PC 3	Year-round operation in second-year ice which may include multi-year ice inclusions
PC 4	Year-round operation in thick first-year ice which may include old ice inclusions
PC 5	Year-round operation in medium first-year ice which may include old ice inclusions
PC 6	Summer/autumn operation in medium first-year ice which may include old ice inclusions
PC 7	Summer/autumn operation in thin first-year ice which may include old ice inclusions

Table 4.3: IACS polar class description

4.2.2 Design ice loads

The design scenario for determining the scantlings required to resist ice loads is a glancing impact on the bow. The design ice load is characterised by an average pressure, P_{avg} uniformly distributed over a rectangular load patch of height, b, and width, w. Within the bow area of all polar class ships, the ice load parameters are functions of the actual bow shape. In order to determine the ice load parameters (P_{avg}, b and w), it is required to compute the following ice load characteristics for sub-regions of the bow area; shape coefficient (fa_i), total glancing impact force (F_i), line load (Q_i) and pressure (P_i). Where i is the sub-region considered, which in this case is the bow.

The force (F), line load (Q), pressure (P) and load patch aspect ratio (AR) associated with the glancing impact load scenario are functions of the hull angles measured at the upper ice waterline (UIWL) in the bow area. The influence of the hull angles is captured through computation of a bow shape coefficient (fa). The hull angles are defined in figure 4.4.

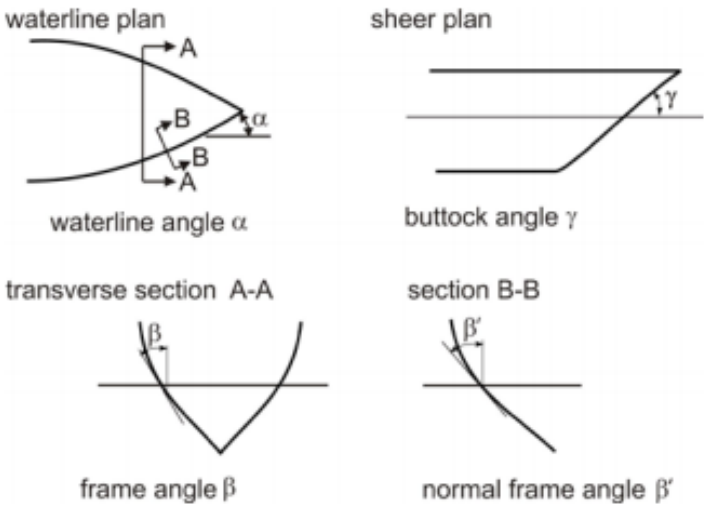

Figure 4.4: Definition of hull angles

The normal frame angle, β', is given as:

$$\beta' = arctan(\frac{sin(\alpha_i)}{tan(\beta_i)}) \tag{4.7}$$

The shape coefficient, fa_i, is to be taken as:

$$\begin{aligned} fa_i &= minimum(fa_{i,1}; fa_{i,2}; fa_{i,3}) \qquad [-] \\ fa_{i,1} &= (0.097 - 0.068(\frac{x}{L} - 0.15)^2) \cdot \frac{\alpha_i}{(\beta_i')^{0.5}} \qquad [-] \\ fa_{i,2} &= 1.2 \cdot \frac{CF_F}{sin(\beta_i') \cdot CF_C \cdot D^{0.64}} \qquad [-] \\ fa_{i,3} &= 0.60 \qquad [-] \end{aligned} \tag{4.8}$$

Where x is the distance from the forward perpendicular (FP) to station under consideration in meters. L is ship length measured on the upper ice waterline in meters. CF_F is the flexural failure class factor, and is equal to 68.6 for PC 1, CF_C is the crushing failure class factor, and is equal to 17.69 for PC 1. D is defined as the ship displacement in [kt] and should not be taken less than 5 [kt].

Force, F_i:

$$F_i = fa_i \cdot CF_C \cdot D^{0.64} \quad [MN] \tag{4.9}$$

Load patch aspect ratio, AR_i:

$$AR_i = 7.46 \cdot sin(\beta') \quad \geq 1.3 \quad [-] \tag{4.10}$$

Line load, Q_i:

$$Q_i = F_i^{0.61} \cdot \frac{CF_D}{AR_i^{0.35}} \quad [MN/m] \tag{4.11}$$

Pressure, P_i:

$$P_i = F_i^{0.22} \cdot CF_D^2 \cdot AR_i^{0.3} \quad [MPa] \tag{4.12}$$

CF_D is the load patch dimensions class factor, and is equal to 2.01 for PC 1.

In the bow area the design load patch has dimensions of width, w_{bow}, and height, b_{bow}, defined as follows:

$$w_{bow} = \frac{F_{bow}}{Q_{bow}} \quad [m] \tag{4.13}$$

$$b_{bow} = \frac{Q_{bow}}{P_{bow}} \quad [m] \tag{4.14}$$

Where:
F_{bow} =maximum force F_i in the bow area [MN]
Q_{bow} =maximum line load Q_i in the bow area [MN/m]
P_{bow} =maximum pressure P_i in the bow area [MPa]

And the average pressure, P_{avg}, within a design load patch is determined as:

$$P_{avg} = \frac{F_{bow}}{b_{bow} \cdot w_{bow}} \quad [MPa] \tag{4.15}$$

4.2.3 Local dimensions

IACS provides a minimum required plate thickness as a function of frame orientation, longitudinal and transverse local frames, web frames and load-carrying stringers. The boundary conditions are assumed fixed for continuous members, and simply supported, unless the boundaries could be proven to provide significantly rotational restraints, for other members. The requirements apply to plating and members directly exposed to ice pressure. Only plating and transverse stiffeners will be further assessed.

The thickness, t, of a plating exposed to ice loads should not be taken less than:

$$t = t_{net} + t_s \quad [mm] \tag{4.16}$$

Where t_{net} is the required plate thickness to resist ice load, and t_s is the corrosion and abrasion allowance. The net thickness for transverse supported plating, where the stiffeners are aligned more than 70 degrees perpendicular to the waterline, is given by:

$$t_{net} = 500 \cdot s \cdot \frac{(\frac{AF \cdot PPF_p \cdot P_{avg}}{\sigma_y})^{0.5}}{(1 + \frac{s}{2 \cdot b})} \quad [mm] \tag{4.17}$$

Where s is the stiffener spacing and l is the length. AF is the hull area factor, which is equal to 1 for the bow area of the PC 1. PPF_p the peak pressure factor depending on the stiffener spacing and is not to be taken less than 1.2 for transversely stiffened plating. σ_y is the minimum upper yield stress of the material in $[N/mm^2]$.

The net effective plastic sectional modulus, Z_p of transverse or longitudinal stiffeners should not be taken less than:

$$Z_p = A_{pn} \cdot \frac{t_{pn}}{20} + \frac{h_w^2 \cdot t_{wn} \cdot sin(\phi_w)}{2000} + \frac{A_{fn} \cdot (h_{fc} \cdot sin(\phi_w) - b_w \cdot cos(\phi_w))}{10} \quad [cm^3] \tag{4.18}$$

A_{pn} is the net cross-sectional area of the local frame in $[cm^3]$, t_{pn} is the fitted net shell plate thickness equal to t_{net}. t_{wn} is the net web thickness that is equal to t_w (built web thickness) without corrosion addition. The remaining parameters are shown in figure 4.5

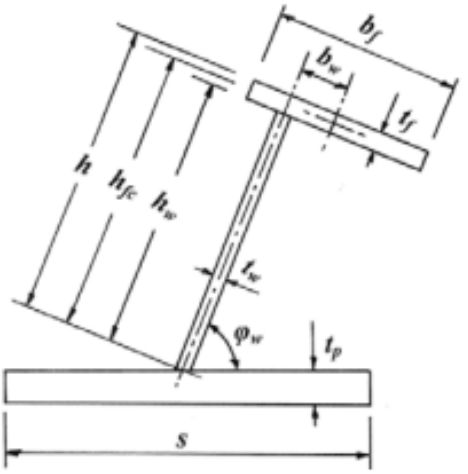

Figure 4.5: Stiffener geometry, IACS (2016)

4.3 Comparison of DNV GL and IACS regulations

In this chapter the main content of the classification rules for ships navigating in ice-infested areas provided by DNV GL and IACS have been presented. The focus was mainly on class notation POLAR-30 and PC 1. DNV GL divides the classes after area of operation, considering Baltic or Polar areas. The classes are given different notations regarding exposed ice thickness and ramming condition. Whereas IACS divides their classes after operational time and expected ice age - strength requirements are based entirely on ice condition regardless of area.

Concerning the ice loads, DNV GL proposes that the local design load depends the design contact area, which equal to 0.4 the ice thickness multiplied with the stiffener span, and ice strength. Correction factors for varying design contact area and reinforced areas are included in the calculations. The calculations of pressure loads depends mostly on the geometry of the local model and the class notation of the vessel. While IACS, on the other side, proposes class factors and shape coefficients that apply to the ice load parameters, the ice load parameters are thus used to obtain the load patch dimensions. The average load patch pressure is then obtained from the ice force divided by the load patch area. The two regulations also provides different load scenarios. DNV GL provides different loading scenarios such as bow impact, beaching, local pressure and compression amidships, whereas IACS only presents bow or non-bow impacts as a design scenario.

Both regulations provides requirements for the plate thickness which consist of a net thickness and a corrosion addition. The net thickness differs in the two regulations, whereas DNV GL includes an aspect ratio and an influence factor, while IACS uses pressure peak factors and area factors. In addition, IACS accounts for the different ratios between stiffener spacing and load heights through parameters for the net thickness. Regarding the sectional modulus, DNV GL provides regulations for the regular sectional modulus, while IACS presents regulations for the plastic sectional modulus. The plastic modulus apply to models where plastic deformations are acceptable. IACS classes are also dependent on ship displacements, while DNV GL classes are independent. Plate thickness and loads are generally higher for IACS class PC 1, compared to DNV GL class POLAR and Icebreaker.

4.4 ISO 19906 for arctic offshore structures

ISO 19906 is an international standard for petroleum and natural gas industries - Arctic offshore structures. It is applicable to offshore structures intended for oil or gas operations in waters that is partially or wholly covered in ice, either seasonally or year-round. The objective of ISO 19906 is to ensure that sub-arctic and arctic offshore structures could pro-

vide an appropriate level of reliability regarding personal safety, environmental protection and asset value to the owner, to the industry and to society in general.

Ice loads refers to local and global ice actions including deterministic and probabilistic methods and dynamic loading. Local actions should, according to ISO 19906, be based on relevant full-scale or established theoretical methods. In addition, the variation in ice properties due to geographical differences should also be taken into consideration.

4.4.1 Floating Structures

Floating systems operating in cold regions and arctic refers to ISO 19904-1, which provides guidance on issues such as hull integrity, hull stability, ice loads and considerations on floaters, station keeping, disconnection and reconnecting, operations, ice detection and management. The requirements and guidance are provided for the operation and design of floating offshore structures to support the following functions:

- Production
- Storage and offloading
- drilling

The system should provide the reliability assumed when computing the the design actions, and be designed for disconnection and reconnecting under the combination of ice and environmental actions relevant for the design situation.

4.4.2 Overview of local ice actions - ISO 19906

While global actions are computed from average pressures over the nominal contact area, there may be many areas within nominal contact area that are subjected to greater local pressures. Due to this, global average pressures should not be used for local designs. Local pressures should be introduced in the design of shell or stiffened elements, see figure 4.6.

When calculating the local load, determining the appropriate load area is a challenge. ISO 19906 has proposed solutions for estimating load area and load. Ice interactions may produce local pressures that can be considered as constant over an area as given by:

$$A = a \cdot w_L \tag{4.19}$$

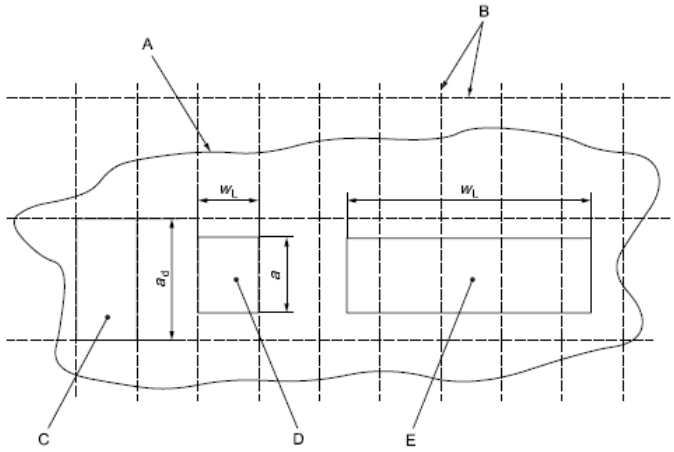

A-global interaction area (grows as interaction proceeds)
B-frames and stiffeners
C-local area for plate design
D-loaded area for plate design
E-loaded area for stiffener design
a-loaded height
a_d-frame spacing
w_L-loaded width

Figure 4.6: Definition of loaded areas for local actions, IACS (2016)

Where a and w_L is the height and width of the loaded area respectively. Maximum action effects usually occur when a equals the height of the local design area, a_d. For level ice, w_L is greater than four times the ice thickness. Local ice pressures differ depending on the thickness of the ice that interacts with the structure.

The local ice actions can be divided into two different categories; first-year thin ice and multi-year massive ice. The relationship between them is, however, based on data-sets with various environmental conditions. As a result, their correspondence is not exact and they might not yield the same local pressures for the same ice thickness. Sound judgement should therefore be used in their application.

4.4.3 Local pressures from thin first-year ice

A method for determining local pressures from first-year ice up to approximately one meter thick. This is a method that applies to level ice, rafted ice and consolidated layers of first-year ice ridges. There exist considerable data from full-scale local pressure measurements for level and rafted ice conditions. Pressure panels have been used to measure the average pressure on an area approximately one meter wide over the full ice thickness.

Local action effects may be assessed by the application uniformly over a local design area of the action, F_L, for a_d greater than 0.14:

$$F_L = 3.72\sqrt{a_d} \cdot w_L \quad [MN] \tag{4.20}$$

Equation 4.20 is valid for $w_L/a_d \leq 10$ and for $a_d \leq 0.4h_E$. Where h_E is the characteristic ice thickness for ELIE. If the height of local design area exceeds $0.4h_E$, the following equations for determine the local actions can be used:

$$\begin{aligned} P_F &= 2.35 \cdot h^{-0.5} \quad [MPa] \qquad for \quad h > 0.35m \\ P_F &= 4.0 \quad [MPa] \qquad for \quad h \leq 0.35m \end{aligned} \tag{4.21}$$

Where h is the ice thickness. P_F is the upper bound value for full thickness pressure.

In a deterministic design, the local pressure on the loaded area is given as:

$$P_L = \gamma_L \cdot P_F \tag{4.22}$$

Where γ_L equals 2.5, and reflects a simplified vertical distribution of the full thickness pressure on the loaded area.

4.4.4 Local ice pressures for thick, massive features

Local pressures due to massive ice features having a thickness that exceeds 1.5 meters can be determined using data shown in figure 4.7. This data have been derived from indentation tests conducted in the Beaufort Sea and from measurements made on the ice pressure panels of the Molikpaq structure in the same area.

The local pressure, p_L, acting on the loaded area can be determined based on these data, as given by:

$$\begin{aligned} p_L &= 7.40A^{-0.70} \quad for \quad A \leq 10m^2 \\ p_L &= 1.48 \qquad for \quad A > 10m^2 \end{aligned} \tag{4.23}$$

Where A is the local design area.

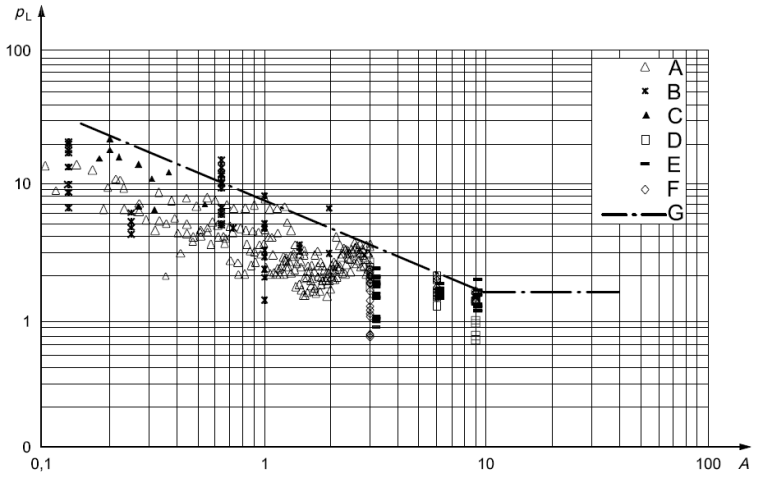

A-3 m^2 Pond inlet test data
B-flat jacket test data
C-1989 Hobson's Choice test data
D-Molikpaq BW data
E-Molikpaq N face data
F-Molikpaq E face data
G-$p_L = 7.40A^{-0.70}$ (mean plus three times the standard deviation)
w_L-loaded width

Figure 4.7: Compilation of data for ice pressures as a function of the loaded area,IACS (2016)

4.4.5 Estimation of local ice loads

In order to estimate the local ice actions, the loaded area is determined at first. The local actions for design of plates and stiffeners depend on the layout of the structure, which will be further discussed in this section.

Plate design

For maximum action effects to be considered, the loaded areas for plate designs can be expressed as $a_d \cdot w_L$ according to ISO 19906, on the basis of DNV GL POLAR-30 ice class requirements with a nominal ice thickness equal to three meters. The width of the loaded area, w_L, is equal to the stiffener spacing, which is 0.6m, and the loaded height, a_d, is equal to 3m, resulting in a loaded area of $1.8m^2$. The local pressure, p_L, is then approximately

$5MPa$ after substituting into equation 4.4.4. The relationship between stiffener spacing and ice pressure can be seen in figure 4.8.

Stiffener design

The loaded area width, w_L, is set to be four times the stiffener spacing. This results in a loaded area of $7.2m^2$, and a local pressure $1.86m^2$ for a stiffener spacing that is 600mm and nominal ice thickness of three meters.

It is interesting to establish the pressure-stiffener spacing relationship in figure 4.8. The local design pressure for both plate- and stiffener design increases with a decreasing stiffener spacing. This indicates that more intensively stiffened panel is expected to have greater pressure capacity.

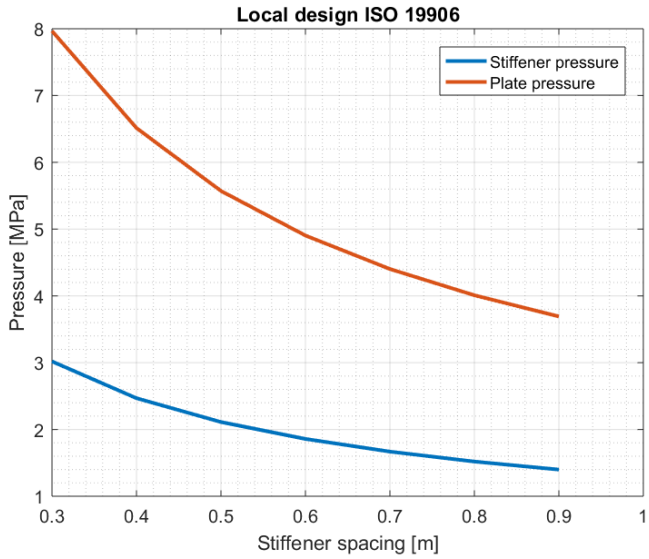

Figure 4.8: Pressure-stiffener spacing curves for plate local design and stiffener local design

Probabilistic model for local ice pressures

A probabilistic local pressure model has been created based on data from ship impacts with multi-year ice floes. The data are mainly from measurements of the Kigoriak ramming tests on multi-year ice, but these are supplemented with data from other vessels as well. The model gives a probability distribution for the maximum annual pressure, p, that corresponds to an annual exposure, μ. The exposure is expressed as a proportion of the average duration

of $0.7s$ for rams in the Kirgoriak trial. The cumulative probability distribution is given by:

$$\begin{aligned} F_p(p) &= exp[-\mu exp(-p/\alpha)] \qquad [MPa] \\ \alpha &= A^{-0.7} \end{aligned} \tag{4.24}$$

This approach is appropriate for a number of discrete impacts per year, and can be applied for multi-year ice interactions and for impact of bergy bits with floating structures.

Chapter 5

Finite Element Method

5.1 General

Finite element method (FEM) is a numerical procedure for analysing structures and continua. FEM is usually applied when the problem addressed is too complicated to be solved satisfactorily by solving the differential equation(s) by classical analytical methods. The results obtained from the FE analyses are rarely exact. However, errors are decreased by processing more equations, and accurate enough results are obtained for engineering purposes at reasonable cost.

The purpose of using FEM is that a complicated solution is approximated by a model that consists of piece-wise continuous simple solutions. FEM models a structure as an assemblage of small parts (elements), where each element is of simple geometry which makes it much easier to analyse the actual structure. All the theory presented in this chapter is obtained from Moan (2003).

5.2 Fundamental laws

FEM is based on following fundamental laws that are used for all structural problems:

- Equilibrium of all parts of the structure (regarding stresses, internal forces).
- Compatibility in the material (regarding displacement-strains).
- Stress-strain relationship (Hooke's law for linearly elastic material).

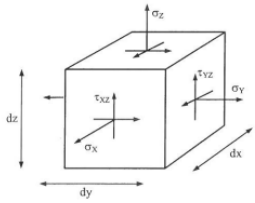

Figure 5.1: Definition of stress on a volume element of a 3D-solid (Moan (2003))

Figure 5.1 represents an infinitely small cube of material with all relevant stress components. In order to get an exact solution to a structural problem, all such small parts of the structure needs to be in equilibrium, point by point. However, plate bending and plane stress (membrane) problems encountered in practice may be difficult to solve. The approximated solution to two and three dimensional structural mechanics problem is rarely exact, but the general idea is that the error in the approximation is reduced with the number of elements that are applied.

5.3 Outline of the method

The analysis of a structure by use of finite element method (FEM) can be divided into distinctive steps, further explained below.

5.3.1 Discretisation

Discretization has a significant effect on the accuracy of the results and is an important effort that has to be done by the structural engineer. Figure 5.2 shows discretization of frame and plane stress problems. For the beam model of a transverse frame, the location of the nodes follow naturally as the joints between physical elements in the structure. For the plane stress problem the geometry of the structure is divided by a mesh into small elements. The elements are connected at points in the corners and along the the edges of each element. The accuracy of the resultas are generally dependent on the number of elements used, or the density of elements.

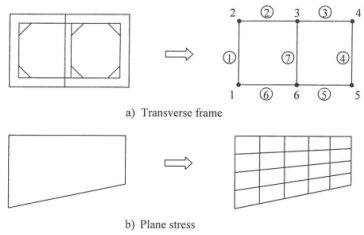

Figure 5.2: Discretization of frame and plane stress problems (Moan (2003))

5.3.2 Element Analysis

The two key components with the element analysis are, maintaining equilibrium of the elements and expressing the displacements within the elements. In addition, stress-strain relationships are needed in order to maintain compatibility.

Shape functions scaled by the node displacements are used to express the displacement within the element. So, by assuming expressions for the shape functions, the displacement in an arbitrary point within the elements is determined by the nodal point displacement. Figure 5.4 illustrates a finite element and its nodal displacements.

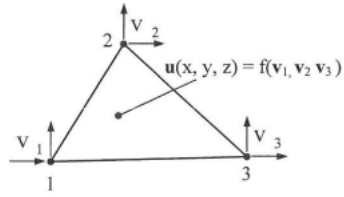

Figure 5.3: Plane stress element (Moan (2003))

Stresses along the edges keep the section that the element is representing in place. It is convenient to work with nodal point forces in the finite element analysis. Equivalent nodal point forces may in the general case replace the edge stresses by demanding the element to be in integrated equilibrium by use of work or energy considerations. This result in a relationship between the nodal point forces and displacements to be given as:

$$\mathbf{S} = \mathbf{k} \cdot \mathbf{v} + \mathbf{S^0} \tag{5.1}$$

Where $\mathbf{S}$ is generalised nodal point forces, $\mathbf{k}$ is the element stiffness matrix, $\mathbf{v}$ is nodal point displacements and $\mathbf{S^0}$ is nodal point forces for external load (fixed end forces). The siffness matrix, $\mathbf{k}$, is obtained in an approximate manner by work or energy considerations.

Computer programs usually have several options for types of elements to choose among. The computer does the work after the analyst has made the choice of element type and loads specified.

5.3.3 System Analysis

By demanding equilibrium for all nodal points in the structure a relationship between the load and the nodal point displacement is established:

$$\mathbf{R} = \mathbf{K} \cdot \mathbf{r} + \mathbf{R}^0 \tag{5.2}$$

$$\mathbf{K} = \sum_j \mathbf{a}_j^T \mathbf{k}_j \mathbf{a}_j \tag{5.3}$$

$$\mathbf{R}^0 = \sum_j \mathbf{a}_j^T \mathbf{S}_j^0 \tag{5.4}$$

$\mathbf{K}$ is the global stiffness matrix, and $\mathbf{R}^0$ are external loads.

5.3.4 Boundary Conditions

The boundary conditions are obtained by setting nodal displacements to known values or by adding spring stiffnesses.

5.3.5 Finding Global Displacement

By solving the linear equations stated above, one can find the global displacement:

$$\mathbf{r} = \mathbf{K}^{-1} \cdot (\mathbf{R} - \mathbf{R}^0) \tag{5.5}$$

5.3.6 Calculation of Stresses

The stresses are computed from the strains by Hooke's law. Strains are computed from the displacement functions within the element combined with Hookes's law. Generally, the stresses are expressed by:

$$\boldsymbol{\sigma}(x, y, z) = \mathbf{D} \cdot \mathbf{B}(x, y, z) \cdot \mathbf{v} \tag{5.6}$$

D is Hooke's law on matrix form, and **B** is derived from the shape functions. The nodal point displacements is given by:

$$\mathbf{v} = \mathbf{a} \cdot \mathbf{r} \tag{5.7}$$

5.4 Linear analysis

In a linear analysis the assumption of small displacements and linear-elastic material behaviour are valid. This implies that there is a linear relationship between the stress and strain.

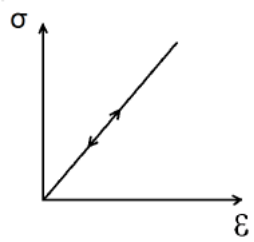

Figure 5.4: Linear relationship between stresses and strains (Moan (2003))

5.5 Nonlinear analysis

When the deformations are large, linear analysis is no longer valid and non-linear analysis has to be applied. The large displacements may cause the structure to change initial geometry after the loads are removed. These impacts on the geometry are difficult to compute and require methods applying iterations to obtain a final result.

5.5.1 Material nonlinearity

For linear analyses, the relationship between stress and strain is assumed to be linear until the stress exceeds a proportionality limit, σ_p. When the stress exceeds this level, the material properties become nonlinear and the relationship between stress and strain are no longer linear, but a function of stress, strain and/or time, illustrated in figure 5.5

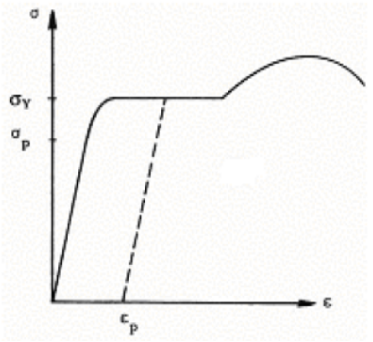

Figure 5.5: Stress-strain curve for mild steel (Moan (2003))

σ_Y is the yield stress. Unloading takes place along the dotted line when the stress reachesσ_y, causing the residual plastic strain, ϵ_p, to remain when stress is removed.

5.5.2 Geometric non-linearity

Geometrical non-linearities are associated with large displacements. In geometrical non-linear problems linear increments replace continuous nonlinear displacements. During deformation the geometry may change and the stiffness, K, will be dependent on the displacement, r, causing the force-displacement relationship to be nonlinear, expressed in equation 5.8. The stiffness consist now of the linear (initial) stiffness, $\mathbf{K_0}$, and the geometrical stiffness, which represents the change in incremental stiffness, $\mathbf{K_G}$, expressed in equation 5.9. The stiffness expressions can be generalised to systems with many degrees of freedom.

$$\mathbf{R} = \mathbf{K}(\mathbf{r}) \cdot \mathbf{r} \tag{5.8}$$

implying

$$\mathbf{K_I}(\mathbf{r})\mathbf{dr} = (\mathbf{K_0} + \mathbf{K_G}(\mathbf{r}))\mathbf{dr} = \mathbf{dR} \tag{5.9}$$

Where **r** and **R** are displacement and load vectors, respectively. Equation 5.9 can be solved by using incremental methods.

5.5.3 Nonlinear boundary conditions

The last non-linearity may be associated with the boundary conditions. Boundary non-linearity occurs when large displacements leads to contact, i.e. when two surfaces come into or out of contact. The stresses and displacements of the contacting bodies are usually not linearly dependent on the applied loads. This type of non-linearity may even occur if the material behaviour is assumed linear and with infinitesimal displacement, due to the fact that the size of the contact area is often not linearly dependent on the applied loads,

i.e. doubling of the applied loads does not necessarily produce double the displacement. A typical non-linear behaviour due to boundaries is illustrated in figure 5.6.

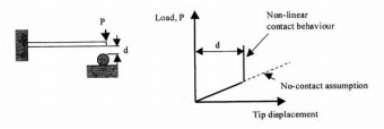

Figure 5.6: Representation of contact (Moan (2003))

5.5.4 Solution techniques

Euler-Cauchy

Several techniques exist for solving these non-linear problems. The *Euler-Cauchy method* is one of them, and is also referred to as the incremental method.

Incremental methods provide a solution by step wise applying the external loading. $\mathbf{\Delta r}$ is determined for each step, and the total displacement is then found by adding each displacement increment. Based on this the incremental stiffness and displacement matrix can be computed. For load increment "m+1" the solution can be determined by:

$$\begin{aligned} \mathbf{\Delta R_{m+1}} &= \mathbf{R_{m+1}} - \mathbf{R_m} \\ \mathbf{\Delta r_{m+1}} &= \mathbf{K_I}(\mathbf{r_m})^{-1}\mathbf{\Delta R_{m+1}} \\ \mathbf{\Delta r_{m+1}} &= \mathbf{r_m} + \mathbf{\Delta r_{m+1}} \end{aligned} \tag{5.10}$$

An improvement of the Euler-Cauchy method, as presented in Moan (2003), may be achieved by an equilibrium correction. The total load and computed displacement are $\mathbf{R_m}$ and $\mathbf{r_m}$ in step "m", respectively. The unbalance between total forces and internal forces may be expressed by the residual force vector:

$$\mathbf{R_r} = \mathbf{R_{int}}(\mathbf{r_m}) - \mathbf{R_m} \tag{5.11}$$

This residual force can be accounted for in the following step, "m+1", as illustrated in equation 5.12. The external loads will be reduced and global equilibrium will be restored.

$$\mathbf{\Delta r_{m+1}} = \mathbf{K_I}(\mathbf{r_m})^{-1}\mathbf{\Delta R_{m+1}} - \mathbf{K_I}(\mathbf{r_m})^{-1}\mathbf{R_r} \tag{5.12}$$

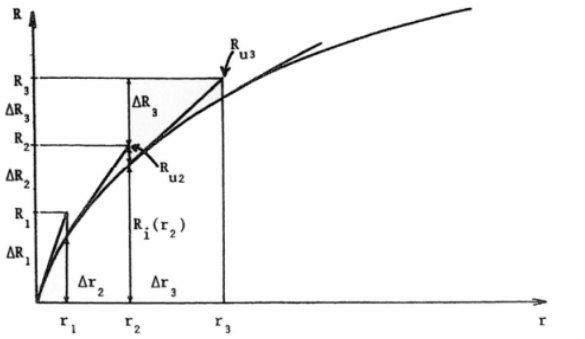

Figure 5.7: Euler-Cauchy procedure with equilibrium correction(Moan (2003))

The additional effort required in this modified Euler-Cauchy method is calculating the internal force vector $\mathbf{R_{int}}(\mathbf{r_m})$.

Newton-Raphson

The most frequently used iterative method for solving nonlinear structural problems is the *Newton-Raphson* method. This method calculates roots by the following formula:

$$x_{n+1} = x_n - \frac{f(x_n)}{f'(x_n)} \tag{5.13}$$

Where $f'(x_n)$ is the derivative of $f(x)$ with respect to x, at $x = x_n$. This method requires that the incremental stiffness matrix, $\mathbf{K}_I$, is established and that $\Delta\mathbf{r}_{n+1}$ is solved from

$$\mathbf{R} - \mathbf{R_{int}} = \mathbf{K_{I(n)}}\Delta\mathbf{r_{n+1}} \tag{5.14}$$

where

$$\Delta\mathbf{r_{n+1}} = \mathbf{r_{n+1}} - \mathbf{r_n} = \mathbf{K_I^{-1}}(\mathbf{r})(\mathbf{R} - \mathbf{R_{int}}) \tag{5.15}$$

in each iterative step. This is thus time consuming, but by updating $\mathbf{K_I}$ less frequently reduced efforts are needed. This method implies only a limited loss of rate of convergence, such *modified Newton-Raphson* iteration is beneficial.

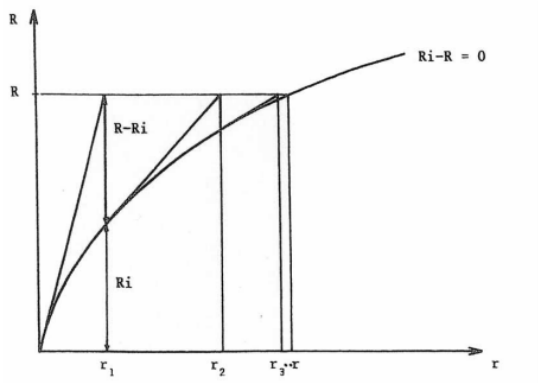

Figure 5.8: Newton-Raphson iteration(Moan (2003))

Advanced solution procedures

Incremental and iterative methods are often combined. The external load is applied in increments and then equilibrium is achieved by iteration in each increment. As long as the load curve are monotonically increasing with displacement, the previous methods described are efficient. However, if there is an extremal point in the load-displacement curves special procedures need to be adopted to achieve acceptable results. Severe difficulties are encountered when load incrementation methods are used to pass a limit point, L, i.e. when the target stiffness becomes zero. Using incrementation in displacement in stead of load may solve this problem. This approach is effective for problems for which the load is uniquely determined by the displacement. However, displacement incrementation will fail at turning point, also known as "snap-back-point".

Arc-length technique is a way for solving these problems. The global equilibrium equation is written as

$$\mathbf{g}(\mathbf{r}, \lambda) = \mathbf{R_{int}}(\mathbf{r}) - \lambda \mathbf{R_{ref}} = \mathbf{0} \tag{5.16}$$

Where $\mathbf{R_{ref}}$ is a fixed external load vector and the scalar λ is a load level parameter. Equation 5.9 defines a state of "proportional loading" in which the loading pattern is kept fixed. The essence of the arc-length method is that the solution is viewed as the discovery of a single equilibrium path in a space defined by the loading parameter, λ and by the nodal variables $\mathbf{r}$. Development of the solution requires a combines incremental (also called predictor) and iterative (also called corrector) approach.

The arc-length is formulated as an additional variable involving both the displacement

and the load. The increment in the load-displacement space may be described by a load increment parameter and a displacement vector Δr, such that $\mathbf{\Delta R} = \mathbf{\Delta}\lambda\mathbf{R_{ref}}$, which is a formulation that results inn an additional equation to be solved. The advantage of the extra equation introduced is that the solution matrix never becomes *singular* even at the limit points. Hence, the solution matrix is re-assembled with $N + 1$ variables, where N is the total number of variables (degrees of freedom) of the system. However, the disadvantage is that in some FE-formulations, the solution matrix becomes unsymmetrical, which can incur an increase in computing time and/or computer storage, particularly for very large problems. Additionally the arc-length method may have some problems with convergence near failure point, but this is usually solved by decreasing the increment size.

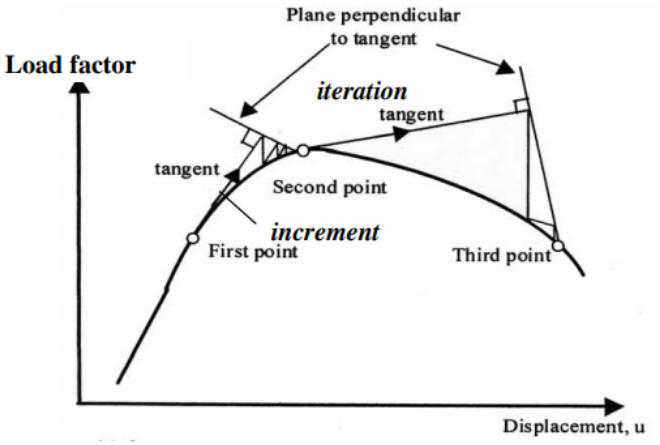

Figure 5.9: Schematic representation of the arc-length technique (Moan (2003))

There exist several methods to obtain the arc length, for example by making the iteration path follow a plane perpendicular to the tangent of the load-displacement curve, as illustrated in figure 5.9.

The methods for directly solving nonlinear problems that are based on incrementation of loads or displacements, and/or combined with iterative methods are usually considered standard methods for solving nonlinear problems (e.g. in ABAQUS).

Chapter 6

Results

FE-models has been established and assessed in order to investigate local ice loads impact on local details of a FPSO-hull. The results in this chapter are based on theory presented in the previous chapters. The established local model will be analysed using ABAQUS, and it is designed by applying measures from DNV GL as presented in section 4.1. Respective local ice pressures from DNV GL and IACS will be assessed, in addition to local ice actions given by ISO 19906.

6.1 Model

Four partly different models will be further analysed and compared with regards to stiffener dimensions and stiffener spacing. All four models are located in the same area of the hull of the FPSO. The local models are based on the SEVAN FPU-ICE which is a floating production and storage for hydrocarbons that is built for operation in ice-infested areas.The SEVAN FPU-ICE has a cylindrical shaped hull that is moored to the seabed. The traditional SEVAN hull to the SEVAN FPU-ICE is modified with a downward sloping cone in the waterline. The inclined conical part of the hull will bend the ice downwards and break it, causing an increase of the draft. The broken ice is pushed down and to the side during ice drifting towards the hull. The draft is on the other hand reduced in open water conditions, moving the conical part out of the water, thus avoiding the effect of nonlinear restoring forces in roll and heave motions.

Figure 6.1: SEVAN FPU-ICE FPSO

The local models will be presented in this section. It was necessary to to some assumptions and simplifications during the computations, but the assumptions were made within reasonable limits trying to fit the actual local model of SEVAN FPU-ICE.

6.1.1 Location of the local model

The models are a section of the conical hull and are located as illustrated in figure 6.2. Figure 6.2 is a structural drawing of the SEVAN FPU-ICE, and is obtained from Huse (2010).

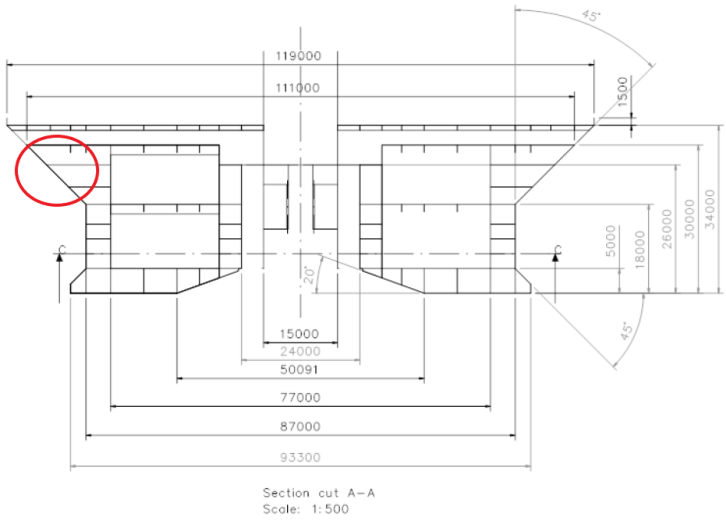

Figure 6.2: Cross section cut

6.1.2 Dimensions

The dimensions of the plate in the model was arbitrarily set to a length of 7m and a width of 2.4m. The following dimensions for the four different models that are presented in table 6.2, were found through calculations applying theory from section 4.1. The width of the plate was arbitrarily chosen to fit the stiffener spacing, and the hull angles were set to 45°, resulting in a web angle, β, equal to 55°. The hull angles are defined in figure 4.3, and the web angle is defined in equation 4.6.

	Abbreviation	Dimension
Stiffener length	l	7000 [mm]
Plate thickness	t	50 [mm]
Section modulus	Z_{min}	642 000 [mm^3]

Table 6.1: Local plate dimensions by application of DNV GL regulations, model 1

The section modulus does not describe the dimensions of the stiffeners, but by application of the section modulus and basic hand calculations, the following dimensions, see table 6.2, for the stiffeners were set:

	Abbreviation	Model 1	Model 2	Model 3	Model 4
Stiffener spacing [mm]	s	600	600	400	400
Web height [mm]	h_{web}	320	460	320	460
Web thickness [mm]	t_{web}	20	20	20	20
Flange height [mm]	t_{flange}	20	-	20	-
Flange width [mm]	w_{flange}	100	-	100	-
Section modulus[mm^3]	Z	707500	705400	707500	705400

Table 6.2: Local stiffener dimensions

Model 1 and 3 have tee-bar stiffeners, while model 2 and 4 have flat-bar stiffeners. The web-height of the flat-bar stiffeners were increased in order to adjust for the decreasing section modulus due to the missing flanges. The section modulus was chosen to be slightly larger than the minimum required by DNV GL. It is desirable to have largest possible section modulus in order to get lower resulting stresses on the stiffened plate.

6.1.3 Established ABAQUS models

By application of the dimensions presented in section 6.1.2, models were established in ABAQUS. The models were assumed to be an out-cut between the vertical stringers and located in the waterline area. They were modelled using S4R elements, with vertically

aligned stiffeners, a horizontal stringer and the out-cut from a deck. For modelling simplifications, the radius was held constant, meaning that the behaviour of the models will be based on a cylindrical hull.

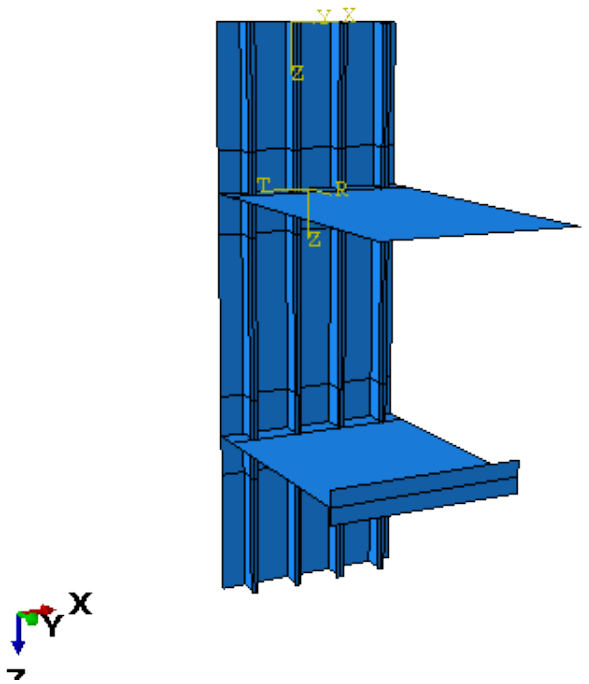

Figure 6.3: Model 1 obtained by DNV GL requirements

All the features of the model are assigned the same material which is high tensile steel EH36. The material properties are shown in table 6.3.

	Abbreviation	Dimension
Young's Modulus	E	204 [GPa]
Poisson's ratio	ν	0.3 [-]
Yield stress	σ_y	355 [MPa]
Density	ρ_s	7850 [kg/m^2]

Table 6.3: Material properties, S355 steel

In order to estimate the plastic behaviour of steel, the material is assumed to behave non-linear. The following stress - plastic strain relation was applied in the material proprieties for plasticity. 355[MPa] defines the initial yield stress, σ_y.

Stress σ [MPa]	Plastic strain ϵ_p
355	0.0
355	0.0174
421	0.1
421	0.15

Table 6.4: Stress-strain from CAE (2013)

Boundary conditions:

The boundary conditions in local model analyses are essential to obtain correct results. The conical hull of the FPU-ICE are exposed to extreme ice loads in the waterline region. In order to get accurate results in the local analyses of the plate fields subjected to extreme ice actions, the effect of the surrounding structure has to be included in the boundary conditions. A common way to apply boundary conditions is by use of symmetry, and is usually used when the loading and structure are symmetrical about the plane.

The boundary conditions are made with a cylindrical datum system due to the conical shape, with radial direction, U1, tangential direction, U2, and vertical direction, U3. The rotation degrees of freedom are UR1, UR2 and UR3 for the respective directions. This implies that six degrees of freedom are considered for this model. The applied boundary conditions for this model are based on boundary conditions obtained from Huse (2010).

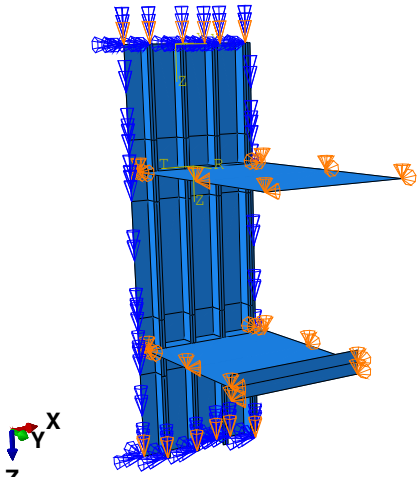

Figure 6.4: Model 1 with applied boundary conditions

The force from the load will go through the plate to the stiffener, and finally thorough the

stringer and deck. The deck and stringer are constrained in tangential and vertical translation (U2=U3=0). Originally, U1 was constrained as well, but due to stress concentrations at the joints of the stringer and plate, and joints of deck and plate, it was necessary to adjust the boundary conditions for the deck and stringer relative to the plate. In this master thesis, the deck and stringer are not the main concern as the focus will dominantly be on the behaviour of the plate and stiffeners.

Furthermore, the vertical edges of the plate are restrained against rotation along the vertical direction (UR3). Finally, the horizontal edges of the stiffened plate, both top- and bottom edges, are constrained against vertical translation and against rotation in all three directions (U3=UR1=UR2=UR3=0).

6.2 Mesh Convergence Study

The size of the applied mesh is an important part in the accuracy of the results of the analysis. It is important to keep in mind that the results are based on numerical values, and that errors may occur due to boundary conditions, modelling errors and material properties when using FEM-programs. A finer mesh will generally give better results as the influence from the errors are reduced, but an increased number of elements also requires larger disk storage and computer central processing units (CPU). It is therefor of great interest to conduct a mesh sensitivity study in order to find a mesh size that gives accurate enough results to a reasonable price.

A mesh convergence study is an excellent way to find the optimal mesh size. In a convergence study one may look at the displacements or stresses that occurs in the model from the applied loads. Stresses generally converge more slowly than displacements, hence it may not be sufficient to only look at displacements. The convergence test was executed by a onset load of 1 MPa over a plate field. Mesh sizes varies between 100 mm to 15 mm, were the mesh size selection generally is based on the half-and-half idea, where the mesh size is decreased twice each time.

A load-displacement and a stress-strain curve was established for the output from the different mesh sizes. The displacement, stress and strain was measured at the centre of the plate and the Load Proportional Factor (LPF) for the whole model was used in order to find the actual load, see section 5.5.4 for information about LPF. One can clearly see in figure 6.5, that the solutions from the arc-length method converges with smaller mesh sizes, resulting in lower displacement and lower loads compared to the greater mesh sizes. The magnitude of the load and displacement were a lot greater for the bigger meshes, and might not be entirely reliable.

The same approach was conducted by comparing the true normal stress-strain relationship in the longitudinal direction for the centre element in the plate field. The stress-strain relationship between the two smallest mesh sizes was almost identical, whereas the relationship for the bigger sizes was very unstable and varied quite a lot.

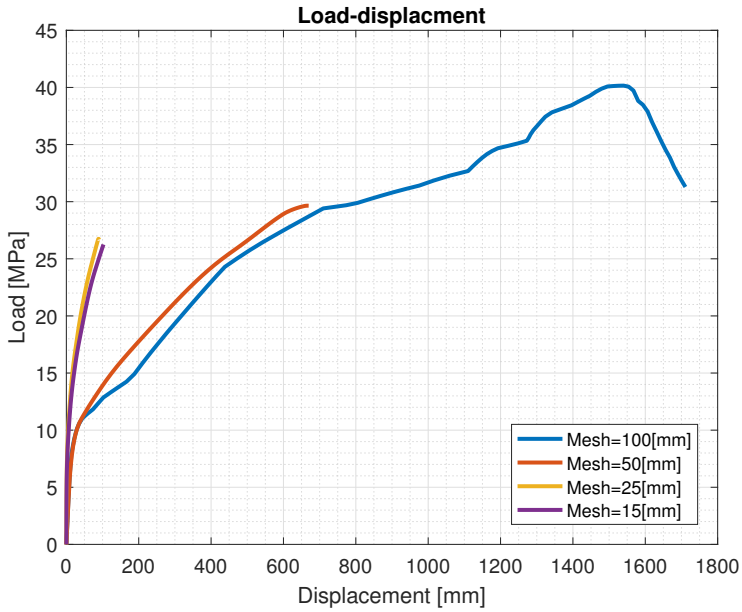

Figure 6.5: Load-displacement curve

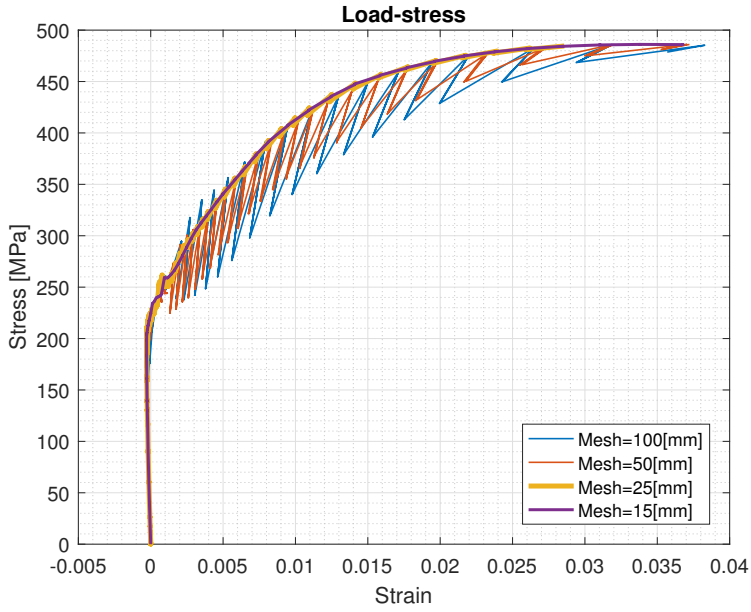

Figure 6.6: True normal stress and true normal strain in longitudinal direction

The difference in the results between the 25mm mesh and the 15mm mesh is not very big. Regarding the models dimensions, the 25mm mesh is an appropriate size, hence this is the size that has been applied in the upcoming analyses.

6.3 The load cases from regulations

The Load case is an applied load-patch between two of the middle stiffeners and between the deck and the stringer, as shown in figure 6.7. Three possible models for computing the local contact pressure from ice have been previously presented in this thesis. These are methods provided by DNV GL, IACS and ISO 19906. The results from the various loads on the four different models will be further assessed in this section.

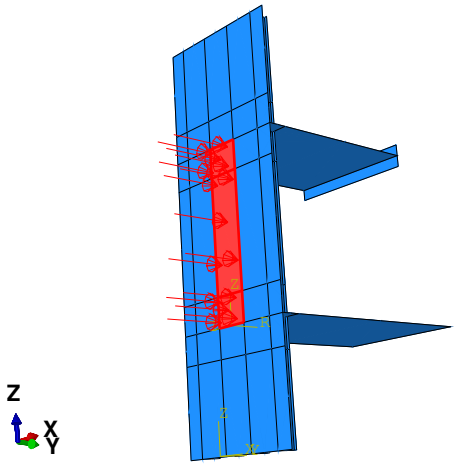

Figure 6.7: Load patch on model

See appendix A, for calculations of the different local pressures. The local ice actions according to DNV GL and ISO 19906 are dependent on the contact area, hence the stiffener spacing. The local contact area is $1.8m^2$ for model 1 and 2, and $1.2m^2$ for model 3 and 4. It is the stiffener spacing that is the changing parameter when computing the local contact area of the ice. The load that is calculated according to ISO 19906 is the massive ice pressure called ELIE, which is short for extreme level ice events.

IACS has a somewhat different approach to obtain the pressure than DNV GL and ISO 19906. The pressure according to IACS is partly dependent on the displacement of the FPSO, a roughly estimation of the displacement of the SEVAN FPU-ICE was conducted based on the sketch in figure 6.2. The average pressure from IACS has been computed based on the assumption that the contact area is kept constant regardless of the applied regulations. This means that the average pressure, P_{avg}, is applied to constant contact areas of $1.8m^2$ and $1.2m^2$ which results in a lower impact force, as IACS suggests a larger contact area equal to $7.46m^2$.

	Local contact pressure [MPa]		
	DNV GL	IACS	ISO 19906
Model 1	5.31	18.5	4.9
Model 2	5.31	18.5	4.9
Model 3	5.64	18.5	6.5
Model 4	5.64	18.5	6.5

Table 6.5: Local contact pressures in [MPa]

6.3.1 Results from load cases from regulations

In this section the von Mises stress, displacement and plastic strain as results from the various local contact pressures provided by DNV GL, IACS and ISO 19906, seen in table 6.5, will be presented for the four models. The objective of these analyses are to see how the stiffened panels are affected by these three different ice loads. The plate with the stiffeners will hence be the main focus of these analyses, hence the results for the deck and stringer will not be further assessed or discusses. The results presented in table 6.6, 6.7 and 6.8 are the maximum values for the plate with stiffeners.

Figures 6.8a, 6.8b and 6.9 show the results from ABAQUS for the von Mises stress, the displacement and the plastic strain for model 1 with applied load according to DNV GL. See appendix A.4 for the results of the analyses of the four different models with applied design load from the different regulations.

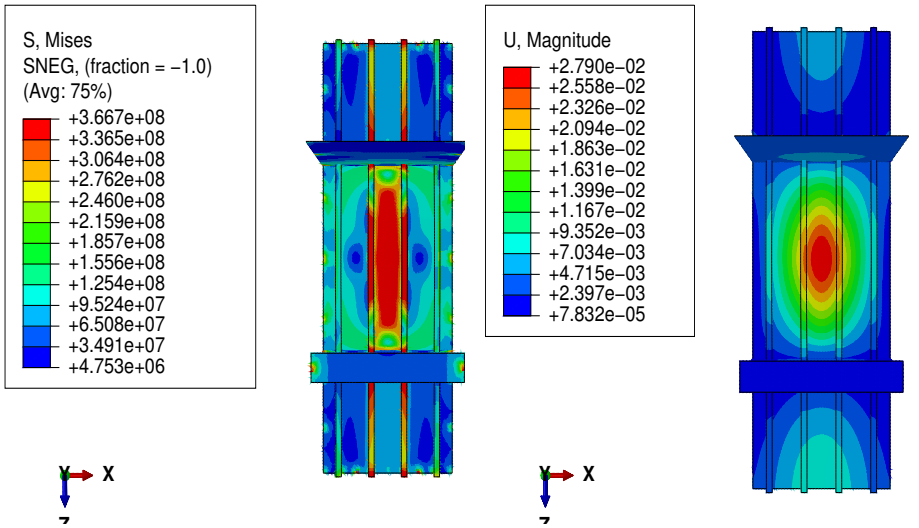

(a) Model 1: von Mises stress for load according to DNV GL

(b) Model 1: Displacement for load according to DNV GL

Figure 6.8

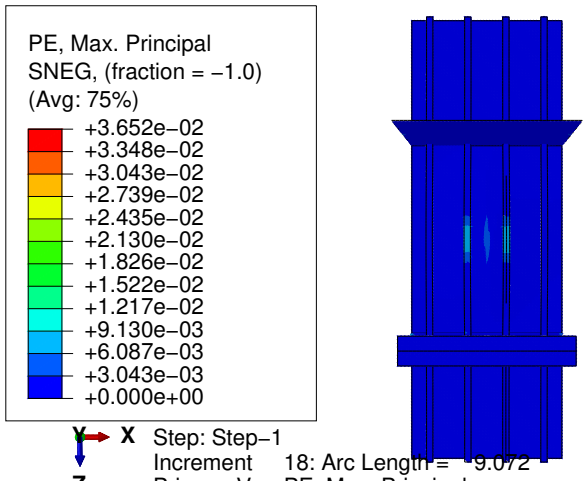

Figure 6.9: Model 1: Plastic strain for load according to DNV GL

Table 6.6 presents the results for the four models with load according to DNV GL regulations. The applied load magnitudes depends on the stiffener spacing. Model 1 and model 2 are exposed to the same load magnitude, and model 2 and model 3 are exposed to another load magnitude.

	von Mises stress [MPa]	Displacement [mm]	Plastic strain
Model 1	366	27.9	0.015
Model 2	386	36	0.0357
Model 3	391	12	0.00484
Model 4	396	10.3	0.00611

Table 6.6: Results from load according to DNV GL

Table 6.7 presents the results for load according to IACS. The same load was applied on the respective load patch for all four models.

	von Mises stress [MPa]	Displacement [mm]	Plastic strain
Model 1	421	478	0.0799
Model 2	421	538	0.107
Model 3	421	216	0.0573
Model 4	421	184	0.073

Table 6.7: Results from load according to IACS

Table 6.8 presents the results for load according to ISO 19906. The decision of the

magnitude of the applied load is also in this case dependent on the stiffener spacing, hence model 1 and model 2 are applied the same load magnitude, and model 3 and model 4 are applied a duplicate load.

	von Mises stress [MPa]	Displacement [mm]	Plastic strain
Model 1	358	24	0.00564
Model 2	397	28.1	0.0138
Model 3	421	17	0.00392
Model 4	421	16.4	0.0853

Table 6.8: Results from load according to ISO 19906

As seen from the results, all the stresses are above yield stress, which is 355[MPa]. This implies that elasto-plastic and plastic behaviour of the material is occurring.

For model 1 and model 3 the highest stresses are located at the top of the middle flanges for all three design loads. The displacement is largest at the centre of the plate where the design load is applied. The plastic strain is largest at the joint of the stiffeners and deck/stringer.

For model 2 and model 4 the maximum stress is located at the top of the middle webs for all three design loads. It is worth mentioning that the difference in the maximum stress magnitude in the webs and the maximum stress magnitude in the plate did not differ much. The maximum displacement is again located in the centre of the plate where the design load is applied. As for model 1 and 3, the plastic strain is largest at the joint of the stiffeners and deck/stringer. The plastic strain is also quite big at the centre of the plate.

6.4 Critical local strain for plate designs

A critical strain analysis has been performed in the centre of the plate between the two middle stiffeners, located as illustrated in figure 6.10. The load was applied in between the two middle stiffeners and between the deck and the stringer, as in figure 6.7. The critical strain analysis has been performed at this location due to the displacement of the plate is at its largest at this location. The object of this This has been done in order to investigate the plate design and to find the maximum load that the plate can withstand before all further deformations are plastic. This critical strain analysis has been conducted on all four models previously presented in this chapter, see the tables 6.1 and 6.2.

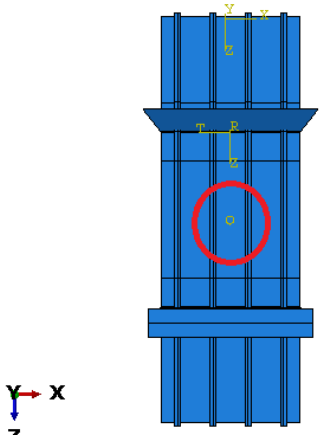

Figure 6.10: Point where the critical strain for plate design have been computed

The maximum principal strain should be less than

$$\epsilon_{crl} \leq \epsilon_{crg}(1 + \frac{5t}{3l}) \tag{6.1}$$

according to DNVGL (2016). Where t is the thickness of the plate, l is the element length in the direction of the maximum principal strain, and ϵ_crg is the critical gross yielding strain. Gross yielding means that plastic deformation with strain above 2% are taking place over a zone $I_{yz} > 20t$ in the direction of the maximum plastic strain. The maximum gross yielding strain in any integration point, in any element within the yield zone, should be limited to the gross yielding critical strain. This critical strain should be found by making a calibration analysis with the actual element type and with an element size relative to the thickness, t, between txt and $5tx5t$. In addition, the gross yielding strain should be determined from deformation limits. The deformation limits for steel plates under out-of-plane bending and membrane tension depends on the yield strength of the steel. In this case the deformation limit in the y-direction is equal to 70mm according to calibration case CC02.

An element size of 100mm was used in order to find the critical gross yielding strain for all four models. This resulted in a maximum principal stress of 0.023 for a displacement equal to 70mm for model 1, which also is equal to the critical gross yielding strain, as illustrated in figure 6.11. See table 6.9 for the results of the critical gross yielding strain and associated critical strains, computed from equation 6.1, for all four models.

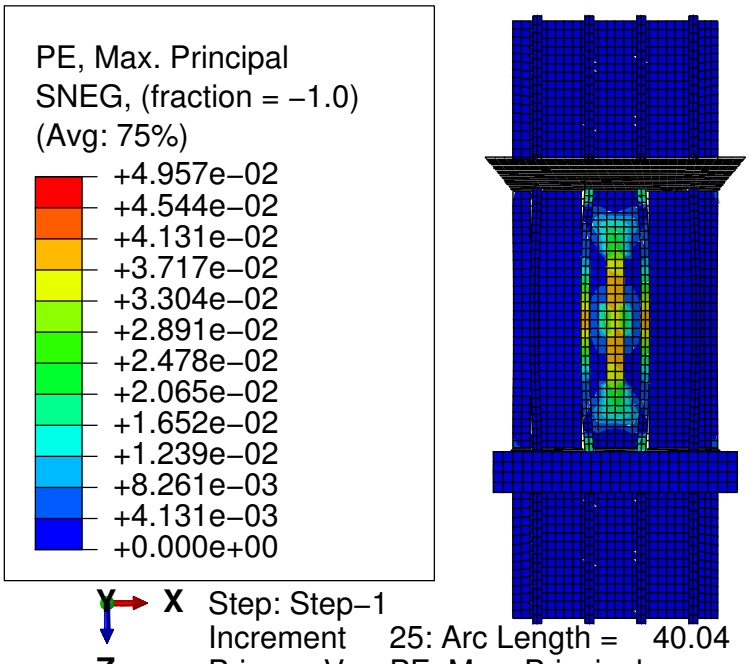

Figure 6.11: Maximum principal strain for a displacement equal to 70mm, Model 1

The element length was set to 100mm, which is equal to two times the thickness, with a thickness of 50mm.

	ϵ_{crg}	ϵ_{crl}
Model 1	0.023	0.0422
Model 2	0.0202	0.0385
Model 3	0.034	0.064
Model 4	0.028	0.051

Table 6.9: Critical gross yielding strain and critical strain for each model

Further the maximum principal stresses and strains in the point of maximum displacement for the four different models was plotted. This was done in order to illustrated the stress-strain behaviour for each model with increasing load. In addition the load-displacement curve has been plotted in the same point. The values used in the two plots are extracted from the results of the non-liner FEM-analyses of the four models conducted in ABAQUS.

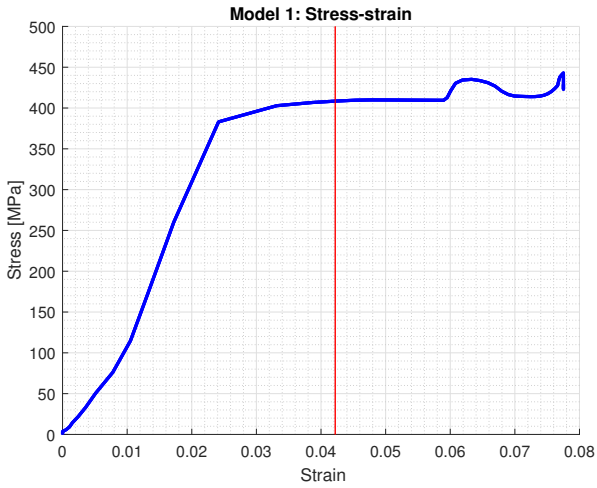

Figure 6.12: Maximum principal stresses and strains, Model 1

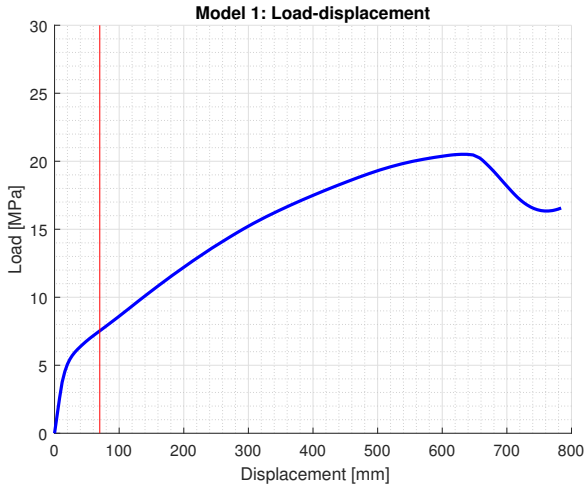

Figure 6.13: Load-displacement, Model 1

The maximum principal strain should, according to DNVGL (2016), not exceed 4.22% for model 1, as this is a critical value. The critical strain is plotted in the figure for maximum principal stresses and strains, see figure 6.14. The associated load that is equivalent to this critical strain is 7.53[MPa]. Strain above this is not recommended by DNV GL, as this would indicate that severe plastic deformations may occur on the structure.

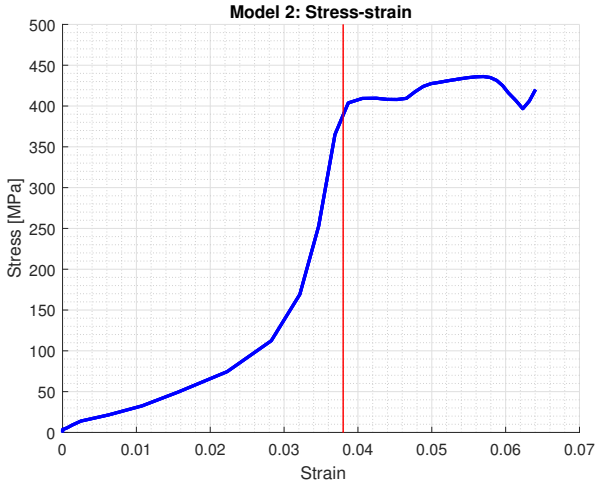

Figure 6.14: Maximum principal stresses and strains, Model 2

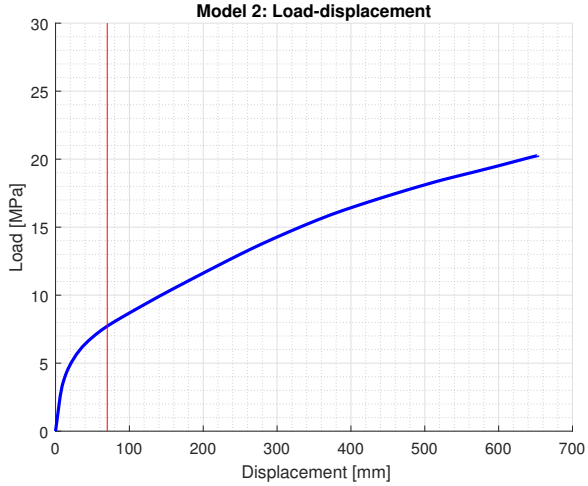

Figure 6.15: Load-displacement, Model 2

The critical strain in model 2 is 0.0385 and is hence less than the critical strain in model 1. The stress-strain curve has a more concave upward shape than the stress-strain curve in model 2. The associated load that is equivalent to this strain is 7.7[MPa].

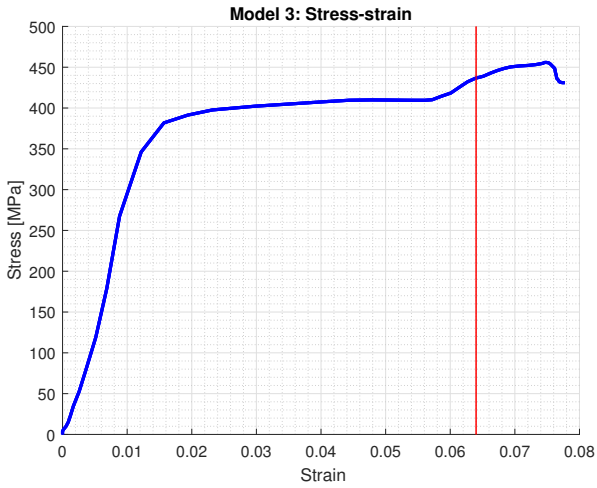

Figure 6.16: Maximum principal stresses and strains, Model 3

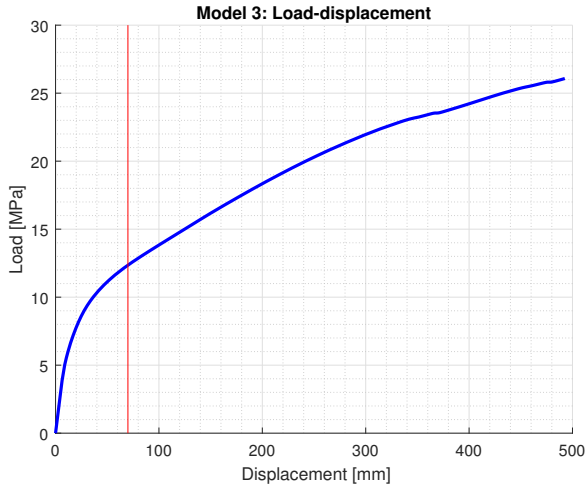

Figure 6.17: Load-displacement, Model 3

For model 3 the critical strain was calculated to be 0.064 according to requirements found in DNVGL (2016). Model 3 has the largest critical strain out of the four models. The load corresponding to this critical strain is equal to 12.3 [MPa].

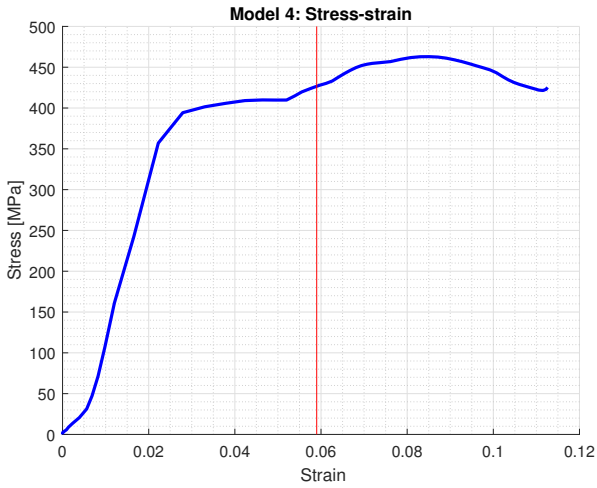

Figure 6.18: Maximum principal stresses and strains, Model 4

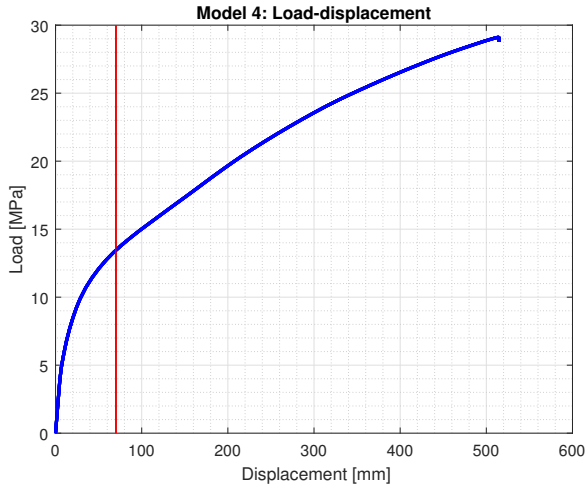

Figure 6.19: Load-displacement, Model 4

For model 4 the critical strain was calculated to be 0.051. This is the second largest critical strain out of the four different ones. The Load corresponding to this strain is equal to 13.3[MPa].

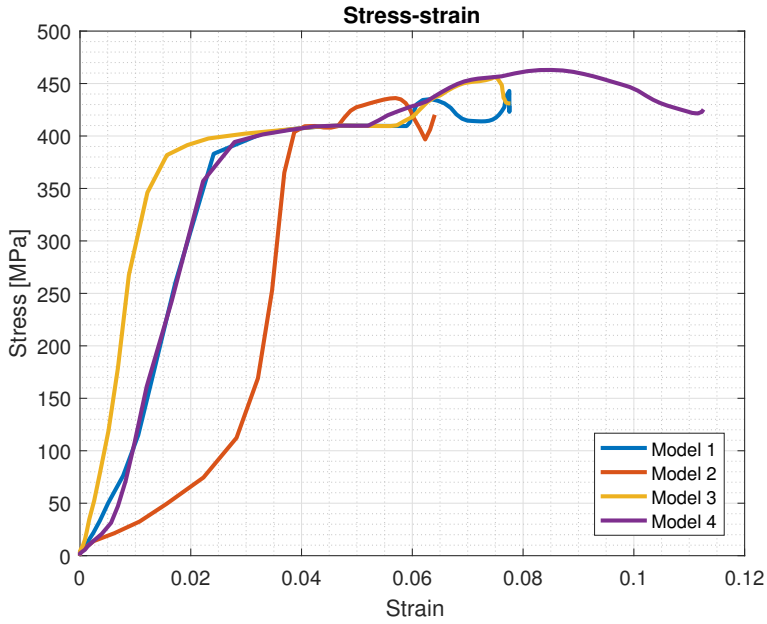

Figure 6.20: Stress-strain for all four models

Figure 6.20 shows the stress-strain for all four models in one plot. This plot has been made in order to easier compare the stress-strain relationship between the four models.

Model 1 and model 4 have a relatively similar behaviour until first yield and through the elasto-plastic area until second yield is reached. All further deformations are then plastic until ultimate strength capacity is reached. Model 2 is the weakest model that clearly reaches the strength capacity of the model first and buckles. Model 3 is the strongest model, and has the longest elasto-plastic area before second yield.

All four models does eventually buckle when the load magnitude is big enough.

Steel becomes brittle at low temperatures. In general materials are qualified at so called "design temperatures", which typically is in the range of 20^oC below minimum expected service temperature. In the Arctic, a minimum service temperature well below -40^oC must be expected, resulting in a minimum design temperature of -60^oC. Large deformations are expected in the Arctic for many reasons like: iceberg collisions, frost heave etc.

6.5 Comparison of critical strain and local design load from regulations

Local design loads have been computed according to methods provided by DNV GL, IACS and ISO 19906, seen in table 6.5. The design loads from DNV GL and ISO 19906 are all less than the critical loads found in section 6.4. The loads provided by DNV GL and ISO 19906 still gives greater von Mises stresses than the yield stress on the structure, implying that the structure will still obtain some plastic deformations, but it should be within somewhat reasonable limits.

The local design load according to IACS, on the other hand, is much greater than all the critical loads obtained in section 6.4. This means that this load will lead to severe plastic deformations.

Chapter 7

Discussion

Regulations
The regulations for model dimensions applied in this thesis were provided by DNV GL and IACS. The class criteria, which is important when deciding local dimensions, are the main difference between these two regulations. DNV GL defines the class notation based on area of operation, the ice thickness and ramming conditions. IACS, on the other hand, defines their classes based on operational time and expected ice age. Operational area is not considered in IACS' regulations.

There are also considerable differences in the method for estimating the local design load between DNV GL and IACS. The local design loads provided by ISO 19906 has also been investigated in this thesis, and will be compared to the methods provided by DNV GL and IACS. The load patch area is one of the input parameters in calculating the local design load using methods provided by both DNV GL and ISO 19906. While the method provided by IACS uses the calculated loads to establish both average contact pressure and contact area. In addition, IACS applies class coefficients that is decided by the vessel class, which in terms were applied in the computations of the design loads. DNV GL and ISO 19906 also applies structural dimensions as a criteria when deciding the local design load, such as the stiffener spacing. The local design loads increases with decreasing stiffener spacing according to DNV GL and ISO 19906. For ISO 19906, the design load increases more with the decreasing stiffener spacing compared to the difference in the design load versus stiffener spacing for DNV GL. For a relative small stiffener spacing, the design load provided by ISO 19906 will be greater than the one provided by DNV GL, but for a relative big stiffener spacing, the design load provided by DNV GL will be greater than the one provided by ISO 19906. This is due to different potency, where the contact area is the base, that are a parameter in computations of local design loads. The design load provided by

IACS was generally much higher than the ones provided by ISO 19906 and DNV GL, with proviso that simplifications were made in order to obtain the local ice actions. One may ask if this is a bit conservative compared to the ones obtained from DNV GL and ISO 19906.

Results from analyses of the four different models with applied design loads
Ice pressures computed from DNV GL, IACS and ISO 19906 were investigated on four different models. The models differs in stiffener dimensions, stiffener space and the amount of stiffeners. Two models consisted of tee-bar stiffener, while the two remaining models consisted of flat-bar stiffeners. The models with the same type of stiffeners had different stiffener spacing, resulting in a different amount of stiffeners on the respective plates. The various stiffener dimensions have a significant effect on the result of the analyses. Consider the results for the different models with applied load from DNV GL, in table 6.6. Model 1 is a tee-bar while model 2 is a flat-bar, and they have equal stiffener spacing. The maximum von Mises stress increased with approximately 5%, the displacement increased with approximately 29% and the plastic strain increased with 138% in Model 2 compared to Model 1. As expected, the stiffener spacing also provided very different results. The stiffener distance increased from 600[mm] for Model 1 to 400[mm] for Model 3. Consequently, the von Mises stress increased with roughly 6%, the displacement decreased with over 50%, and the plastic strain decreased with over 70%.

Naturally, the three different ice pressure gave different stresses, displacements and strain in the stiffened plates as the magnitude of the loads differs. All three design loads resulted in a maximum von Mises stress greater than the yield strength, implying that some plastic behaviour will occur. The stress-strain relationship will no longer be linear, consequently, a relative small increase of stresses may cause large displacements.

Local critical strains
The local critical strain, according to DNVGL (2016), were computed for each of the four different models regarding plate design. The local critical strain was computed from the critical gross yielding which is equal to the maximum principal strain for a given displacement. The models with tee-bars stiffeners had a greater critical gross yielding strain, hence a greater critical strain, than the models with flat-bar stiffeners. In addition, the number of stiffeners also have an impact on the principal stresses and strain. This is as expected as the flanges in the tee-bars can absorb more stresses than the flat-bar stiffeners, and hence withstand greater external loads. In addition, a decreasing stiffener space that resulted in an increased number of stiffeners had a significant effect on both the critical gross yielding strain and critical strain. With an increased amount of stiffeners, the local critical strain increased, implying that the model can resist greater loads. This was also as expected as multiple stiffeners will obtain more stresses as well.

Boundary conditions and mesh size

In order to obtain correct and accurate results, the boundary conditions and mesh size need to be correct. The mesh size was decided from a mesh convergence study to be 25[mm]. This should, according to the convergence study, be an appropriate mesh size that will provide accurate enough results without using to much computational time and storage on the computer. The results on the plates with the applied boundary conditions seem to give reasonable results, but the boundary conditions on the stringer and deck was not sufficient. High stress concentrations occurred in the boundary conditions along the stringer and deck. However, since the deck and stringer was not the main focus in this thesis, this issue was neglected.

Chapter 8

Conclusion

Several topics have been presented and investigated throughout this thesis, with main focus on ice properties, regulations and ice loading. This conclusion is a summery of the most important aspect in each part of the thesis.

The most important features of sea ice that affects marine operations are the amount of sea ice present, ice thickness, the geometry of the ice and movement of ice. Parameters that strongly influence the strength of the ice are; the ice thickness, density, porosity, temperature and grain size and direction. These parameters are important when determining the ice strength.

The regulations provided by DNV GL and IACS are based on different sea ice observations and model tests. They have different methods for computing the local contact pressure, hence their prediction of the contact pressure do differ. In addition, the safety factors and coefficients applied in their respective equations are different. Hence, the two regulations provided very different contact pressures in magnitude. ISO 19906, on the other hand, provided a contact pressure more similar to the one obtained using DNV GL. This is due to the estimation of contact area, which is partly dependent on the stiffener spacing in both regulations. The contact area is used in the computations of local contact pressure for both DNV GL and ISO 19906 regulations. One could assume ice pressure from IACS regulations and either DNV GL or ISO 19906 regulations to account for any uncertainties in the ice-structure interaction model. But, regarding the difference in pressure levels provided by IACS and DNV GL/ISO 19906, it is reason to believe that the design loads given by IACS are generally higher than the ones provided by DNV GL or ISO 19906,

when considering the ice classes PC 1 and POLAR 30.

The interaction models between offshore structure and ice are simplified models. Further, the load contact area was simplified and given a fixed value, even though the contact area will have temporal variations. Defining length and height of the contact area is difficult in such a model. The interaction model provides an estimate of one ice-structure interaction, but for an offshore structure located in ice-infested areas, the number of interactions depend on the ice concentration, and can typically be very large. Additionally, one may assume that the pressure condition may occur once during life-time operation, but it is not necessarily a representation of the conditions presented by a the sea ice data sets.

Non-linear finite element analyses was conducted on four different models in ABAQUS. The applied loads from regulations were all above yield strength, causing plastic behaviour. Plastic behaviour implies that stresses and strains no longer will have a linear relationship, meaning that small changes in stresses will potentially result in large variations off the displacement. The stiffener dimensions, stiffener spacing and amount of stiffeners are important parameters in strength analyses. The results from the assessment indicate that the dimensions applied on the stiffened plates to be a minimum requirement from the classification societies. Considering the magnitude of pressure induced to the models, the stiffener dimensions should have been larger and the stiffener spacing should be relative narrow. In addition, to withstand the applied pressures, the model should have a thicker plate. But by increasing all the model dimensions, the weight and cost of the structure will increase as well, and should be kept in mind.

The critical strain for the plate design was computed for each model according to DNVGL (2016). The critical strain increased with decreasing stiffener spacing and larger stiffener dimensions. The loads given by DNV GL and ISO 19906 were both within the critical strains, while the load provided by IACS provided plastic strain much greater than the critical strain. If it is desirable to make a model where the maximum principal plastic strains are less than critical strain for loads with magnitude according to IACS, the thickness of the plate and stiffener dimensions need to be increased, in addition to having a narrow stiffener spacing. The local critical strain is also very much dependent on the temperature, as steel becomes more brittle with decreasing temperatures, implying that the material should be qualified at so-called "design temperatures". In addition, larger deformations/strains are expected in Arctic for several reasons: frost heave, collisions with icebergs etc.

Chapter 9

Further work

Recommendations for further work would be to investigate the stress-strain relationship and load-displacement relationship for the stiffener designs. This could be done by applying a larger patch load on the model, that for instance is four times the stiffener space, as mentioned in section 4.4.2.

Further work could also be to build a larger substructure for a more accurate simulation. Applying correct boundary conditions that will give realistic results can be a challenge in local models. The more realistic boundary conditions, the better the results. Stress concentrations appeared in the joints of the model due to the boundary conditions and in the nodes along the edged on the deck and stringer where a boundary condition was applied. These should be further investigated and modified in order to obtain better results. One could also run the analyses with Cartesian coordinate, and compare with the analyses that has cylindrical coordinates. The local model is quite small compared to the full size structure, and cylindrical coordinates may not be necessary.

When computing the ultimate strength analysis, imperfections of the structure could be introduced for more reliable results. The dimensions and geometry of the models in ABAQUS are exact, but this is usually not the case in real life, this would be accounted for by introducing geometrical imperfections. This could be performed by using eigenmodes for linear buckling.

An extensive parameter study could also be conducted in order to optimise the design. This could for instance be a further parameter study of the stiffener dimensions, where the web height and thickness, and flange height and thickness are further assessed. In addition, different stiffener shapes, like angle-bar or bulb-flat stiffener, may be applied and further

investigated.

Bibliography

Blanchet, D., C. A. F. J., Badra-Blanchet, P., 1989. An Analysis of Observed Failure Mechanisms for Laboratory, First Year and Multi-Year Ice Working Group. CRRL special report.

CAE, 2013. Using stress-strain data in a finite element simulation.
URL https://caeai.com/blog/using-stress-strain-data-\finite-element-simulation

Cox, G. F. N., Weeks, W. F., 1983. Equations for determining the gas and brine volumes in sea-ice samples.

DNVGL, 2013. Ships for navigation in ice.
URL https://rules.dnvgl.com/docs/pdf/DNV/rulesship/2011-01/ts501.pdf

DNVGL, 2016. Determination of structural capacity by non-linear finite element analysis methods.
URL http://rules.dnvgl.com/docs/pdf/dnvgl/RP/2016-09/DNVGL-RP-C208.pdf

Huse, V., 2010. Analysis and design of the Sevan FPSO against abnormal ice actions. Department of Marine Technology, Norwegian University of Science and Technology.

IACS, 2016. Requirements concerning POLAR CLASS. IACS.

ISO 19906:2010, N.-E., 2014. Petroleum and natural gas industries
arctic offshore structures.

Løset, S., S. K. N. G. O. T., Høyland, K. V., 2006. Actions from ice on Arctic offshore and coastal structures. Lan.

Moan, t., 2003. Finite Element Modelling and Analysis of Marine Structures. Department of Marine Technology, Norwegian University of Science and Technology.

Palmer, A., Croasdale, K., 2013. Arctic Offshore Engineering. World Scientific Publishing Co Pte Ltd.

Sand, B., 2008. Nonlinear finite element simulations of ice forces on offshore structures. Department of Civil, Mining and Environmental Engineering, Division of Structural Engineering, LuleÃě University of Technology.

Stephan, B. J., 2017. Ice Loading on Ship Hull. Department of Marine Technology, Norwegian University of Science and Technology.

Timco, G., Burden, R., 1996. An analysis of the shapes of sea ice ridges.

WMO, 2006. Sea-ice information services in the world, edition 2006.
URL https://library.wmo.int/pmb_ged/WMO_574%5B1%5D.pdf

WMO, 2017. Sea-ice information services in the world, edition 2017.
URL https://nsidc.org/sites/nsidc.org/files/files/noaa/iicwg/2017/WMO_574_Sea_Ice_Information_Services_in_the_World_20170802.pdf

Appendix A

Assessment of ice pressure

A.1 DNV GL

Contact pressure between the stiffeners; F_A equals 1 and σ_{ice} is equal to 10[MPa]:

$$p = F_B \cdot 10000 \qquad [kPa] \tag{A.1}$$

$$\begin{aligned} F_B &= \frac{0.58}{(A_C)^{0.5}} \qquad for \quad A_c \leq 1.0m^2 \\ &= \frac{0.58}{(A_C)^{0.15}} \qquad for \quad A_c > 1.0m^2 \end{aligned} \tag{A.2}$$

$h = 3m$ - distance between stringer and deck.
s- stiffener spacing
A_C - contact area

	$A_c = h \cdot s[m^2]$	Contact pressure [kPa]
Model 1	1.8	5310
Model 2	1.8	5310
Model 3	1.2	5643
Model 4	1.2	5643

Table A.1: Contact pressure between the stiffeners

A.2 IACS

The procedure of calculations of ice actions are based on theory presented in section 4.2. The volume of the SEVAN FPU-ICE was estimated to be approximately 200 000m^3 based

on figure 6.2. By demanding equilibrium between the buoyancy and Newtons 2. law; $O = \rho_{seawater} \cdot g \cdot V_{submerged-volume} = m \cdot g$. The displacement was roughly estimated to be approximately 205[kt]. Based on this displacement and the normal frame angle (see equation A.3), the shape coefficient was calculated and estimated to be $fa = 0.26$.
The following results for the force and pressure is then:

$$\beta' = arctan(\frac{sin(45°)}{tan(45°)}) = 35° \tag{A.3}$$

$$F = fa \cdot CF_C \cdot D^{0.64} = 0.26 \cdot 17.69 \cdot 205^{0.64} = 138.7 \quad [MN] \tag{A.4}$$

By applying the flexural failure class factor $CF_D = 2.01$, and a load patch aspect ration $AR = 4.3$, the linear Q load and pressure P is obtained:

$$Q = F^{0.61} \cdot \frac{CF_D}{AR^{0.35}} = 138.7^{0.61} \frac{2.01}{4.3^{0.35}} = 24.4 \quad [MN/m] \tag{A.5}$$

$$P = F^{0.22} \cdot CF_D^2 \cdot AR^{0.3} = 138.7^{0.22} \cdot 2.01^2 \cdot 4.3^{0.3} = 18.5 \quad [MPa] \tag{A.6}$$

The average pressure is then obtained by the following equation:

$$P_{avg} = \frac{F}{w \cdot b} = \frac{F}{\frac{F}{Q} \cdot \frac{Q}{P}} = 18.5 \quad [MPa] \tag{A.7}$$

A.3 ISO 19906

Local pressure from thick massive ice based on the same contact area as calculated in A.1.

$$p_L = 7.40A^{-0.70} \quad for \quad A \leq 10m^2 \tag{A.8}$$

	$A_c = h \cdot s[m^2]$	Contact pressure [MPa]
Model 1	1.8	4.9
Model 2	1.8	4.9
Model 3	1.2	6.5
Model 4	1.2	6.5

Table A.2: Contact pressure between the stiffeners

A.4 Results for load case from regulations

A.4.1 Model 1

IACS

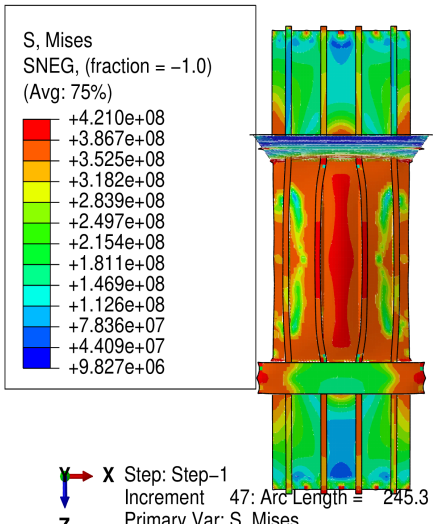

(a) Model 1: von Mises stress for load according to IACS

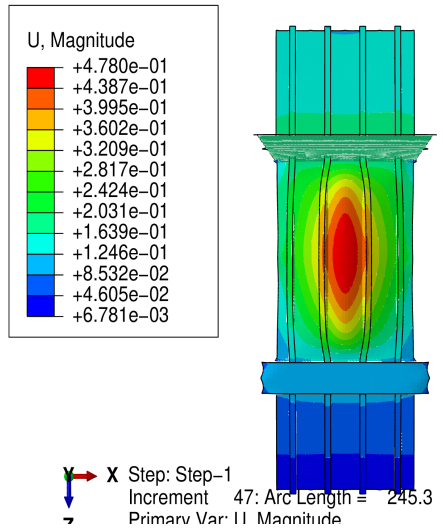

Model 1: Displacement for load according to IACS

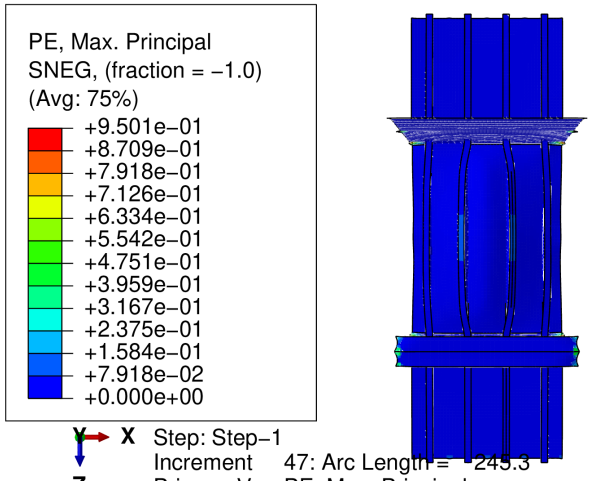

Figure A.2: Model 1: Plastic strain for load according to IACS

ISO 19906

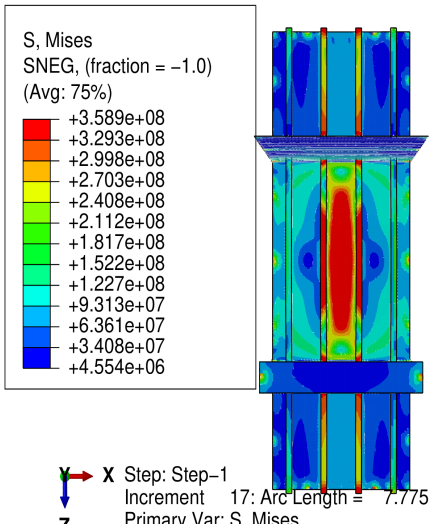

(a) Model 1: von Mises stress for load according to ISO 19906

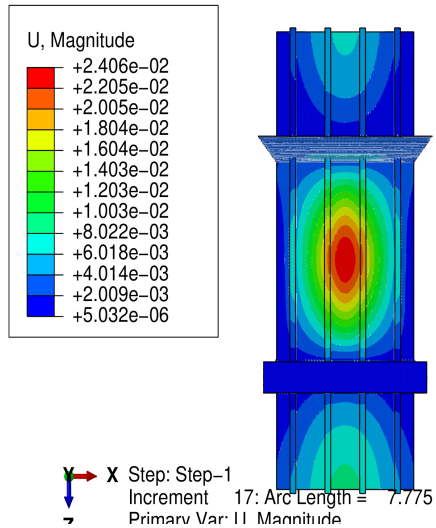

(b) Model 1: Displacement for load according to ISO 19906

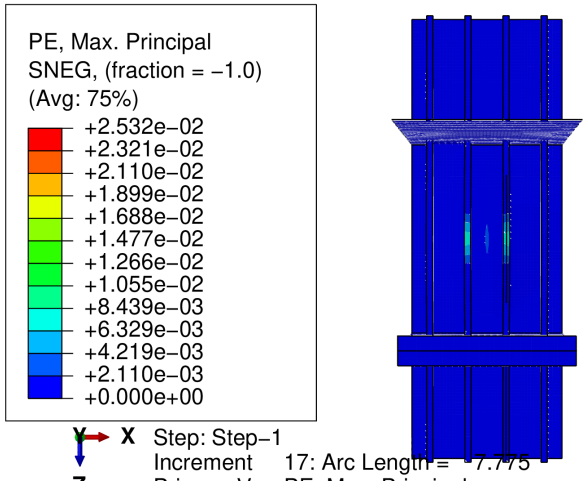

Figure A.4: Model 1: Plastic strain for load according to ISO 19906

A.4.2 Model 2

DNV GL

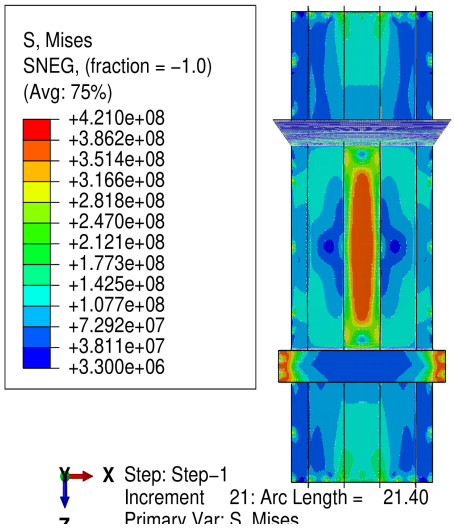

(a) Model 2: von Mises stress for load according to DNV GL

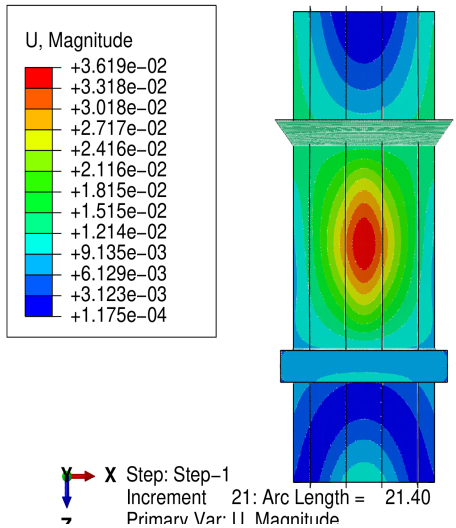

(b) Model 2: Displacement for load according to DNV GL

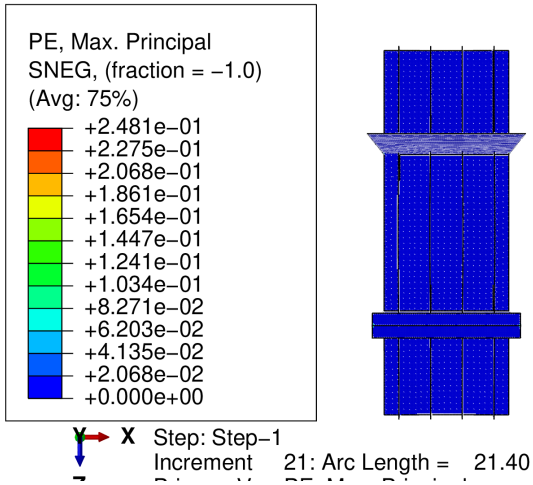

Figure A.6: Model 2: Plastic strain for load according to DNV GL

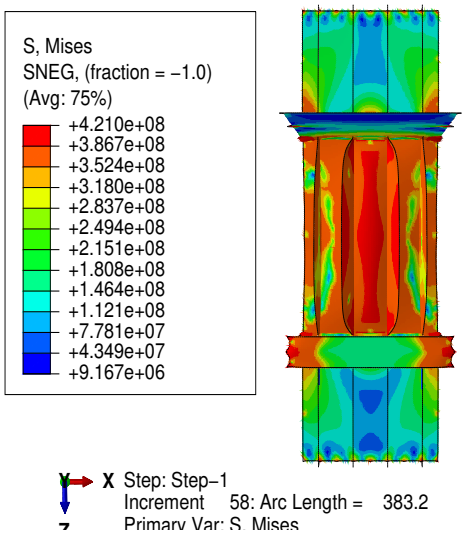

(a) Model 2: von Mises stress for load according to IACS

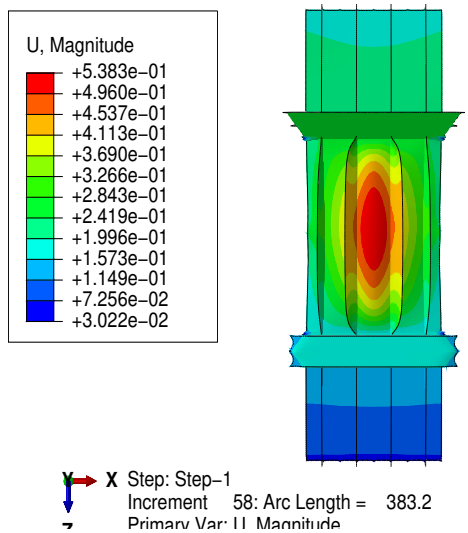

Model 2: Displacement for load according to IACS

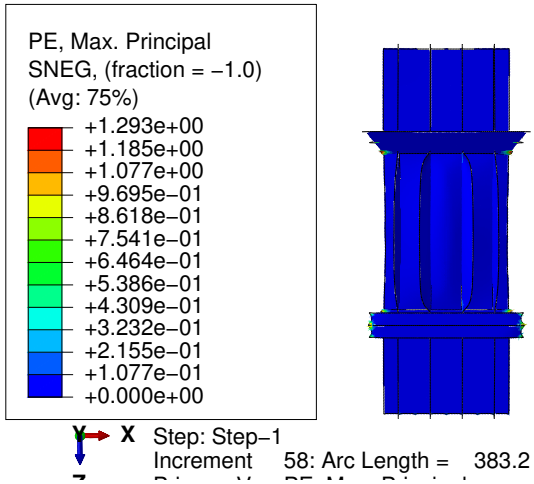

Figure A.8: Model 2: Plastic strain for load according to IACS

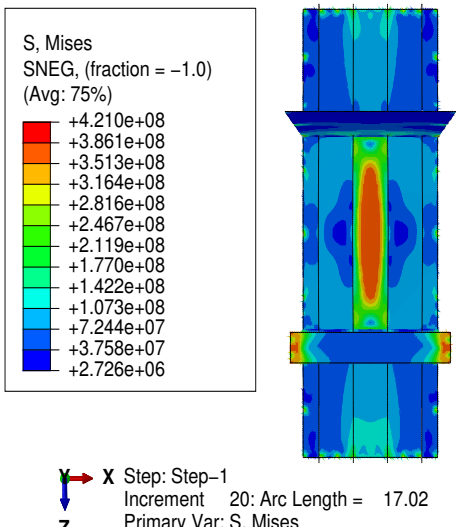

(a) Model 2: von Mises stress for load according to ISO 19906

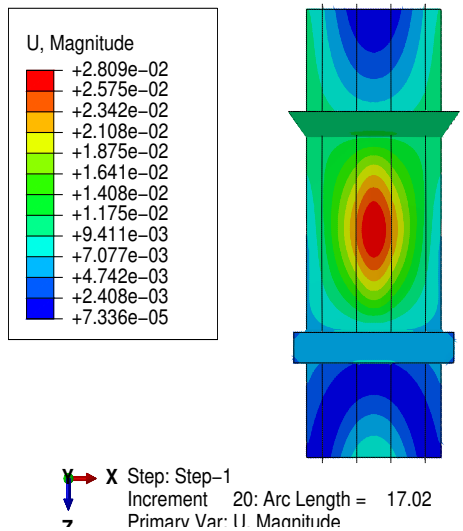

(b) Model 2: Displacement for load according to ISO 19906

Figure A.9

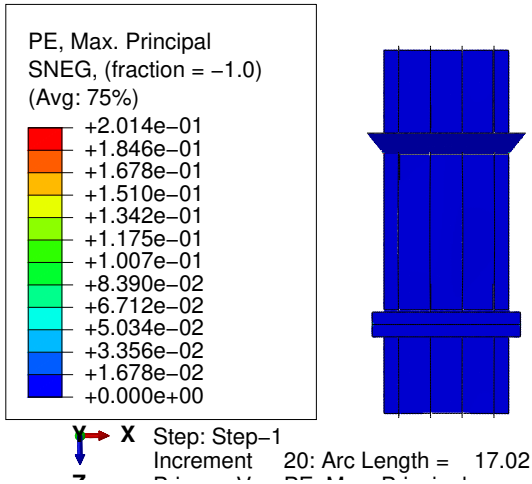

Figure A.10: Model 2: Plastic strain for load according to ISO 19906

A.4.3 Model 3

DNV GL

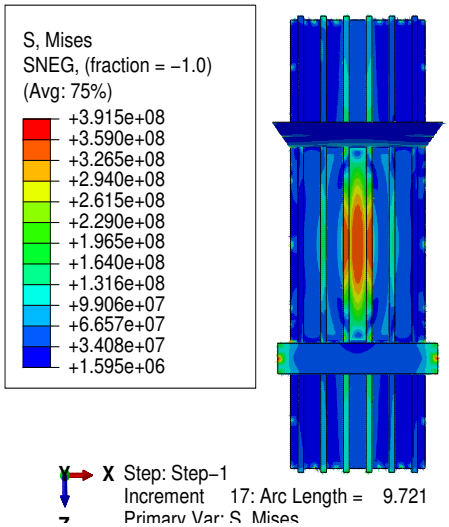

(a) Model 3: von Mises stress for load according to DNV GL

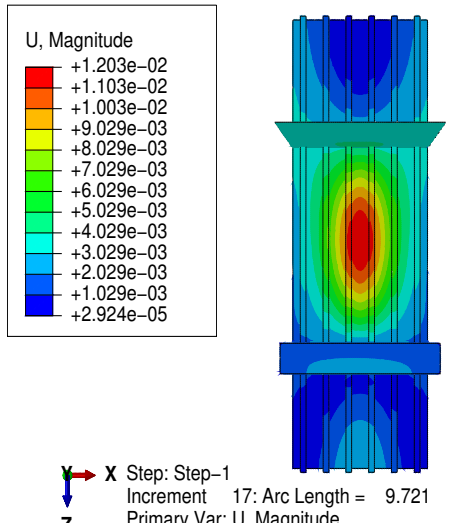

(b) Model 3: Displacement for load according to DNV GL

Figure A.11

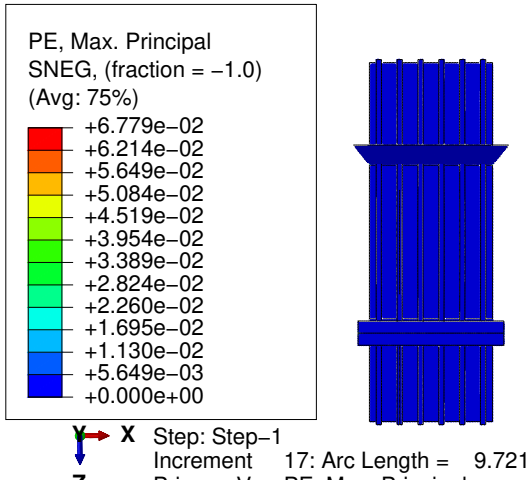

Figure A.12: Model 3: Plastic strain for load according to DNV GL

IACS

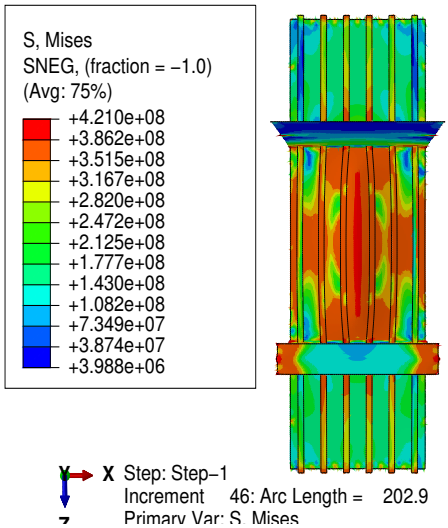

(a) Model 3: von Mises stress for load according to IACS

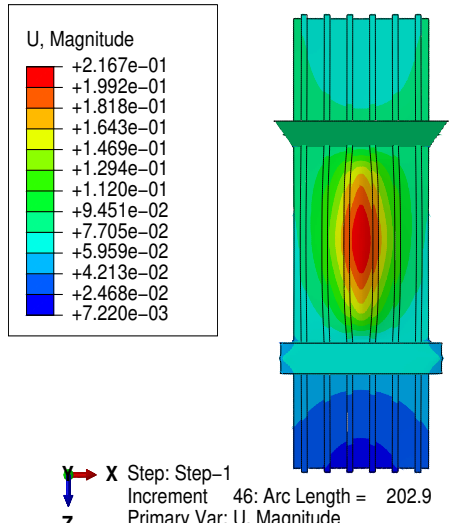

Model 3: Displacement for load according to IACS

Figure A.13: Failure modes ISO 19906:2010 (2014)

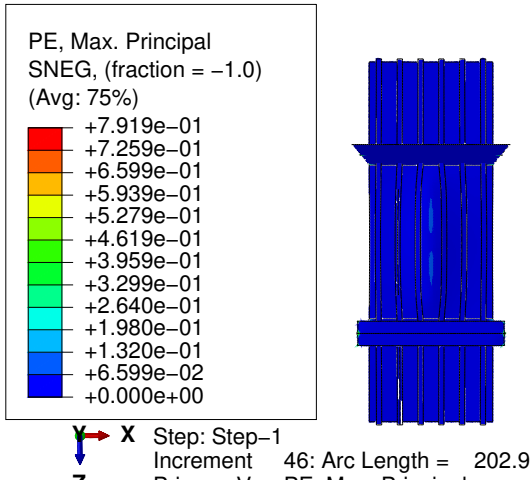

Figure A.14: Model 3: Plastic strain for load according to IACS

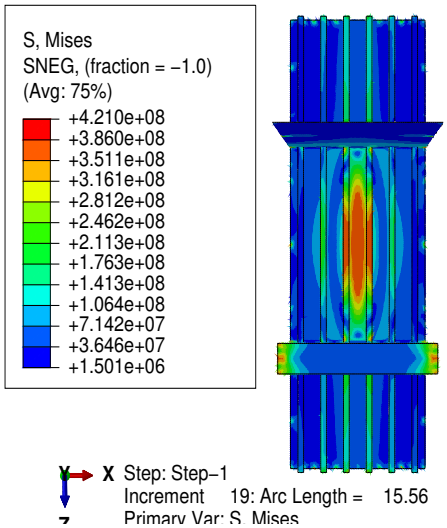

(a) Model 3: von Mises stress for load according to ISO 19906

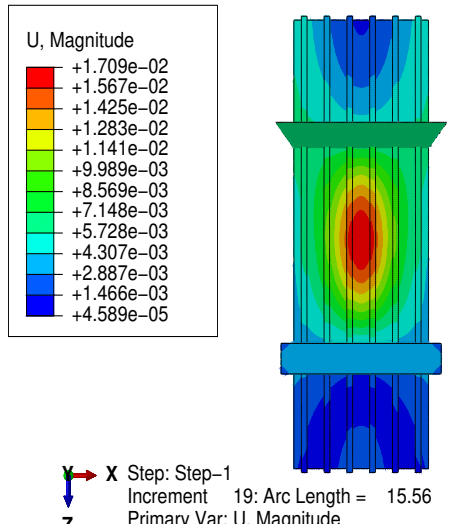

(b) Model 3: Displacement for load according to ISO 19906

Figure A.15

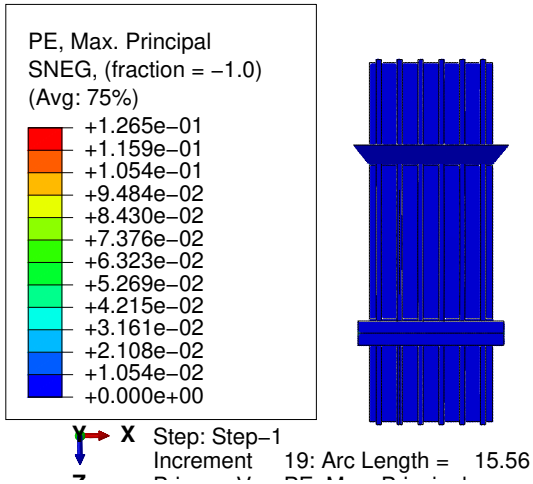

Figure A.16: Model 3: Plastic strain for load according to ISO 19906

A.4.4 Model 4

DNV GL

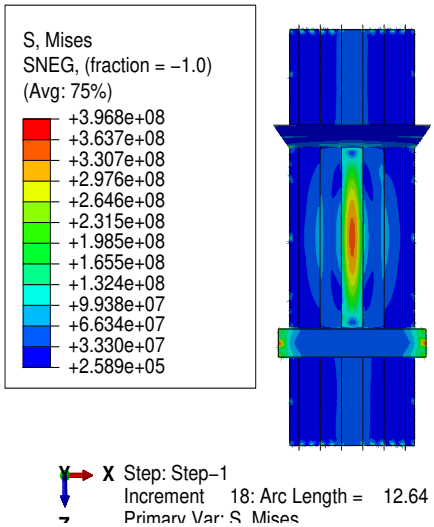

(a) Model 4: von Mises stress for load according to DNV GL

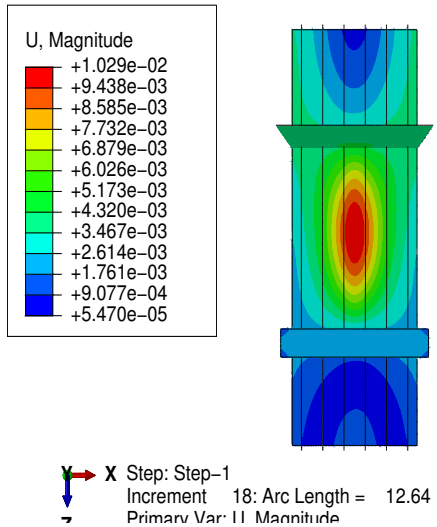

(b) Model 4: Displacement for load according to DNV GL

Figure A.17

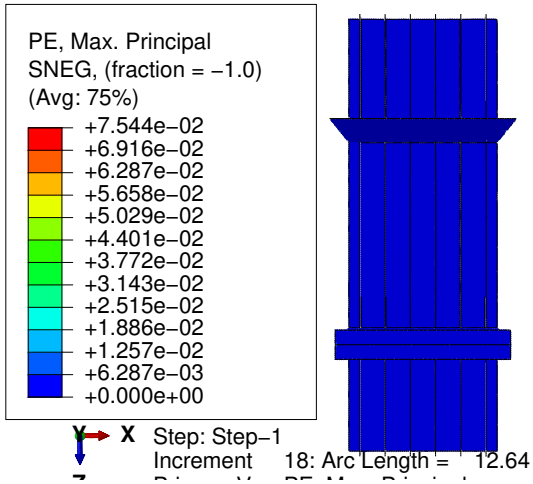

Figure A.18: Model 4: Plastic strain for load according to DNV GL

IACS

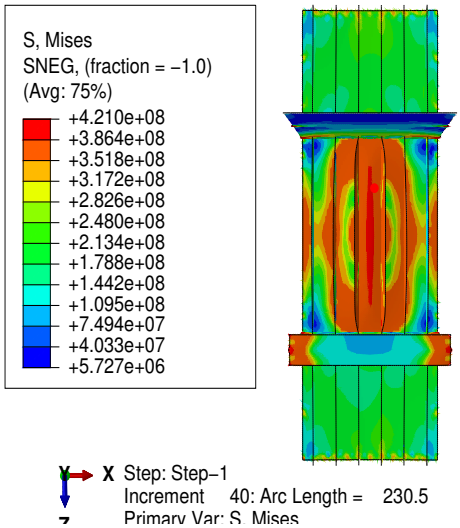

(a) Model 4: von Mises stress for load according to IACS

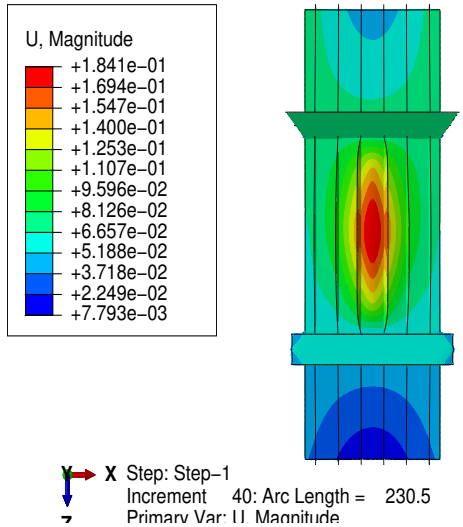

Model 4: Displacement for load according to IACS

Figure A.19: Failure modes ISO 19906:2010 (2014)

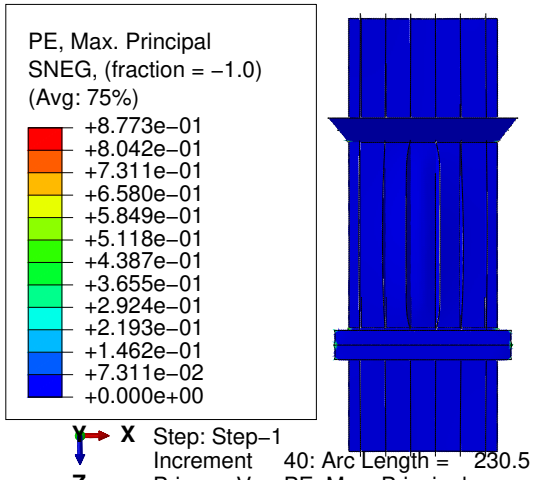

Figure A.20: Model 4: Plastic strain for load according to IACS

ISO 19906

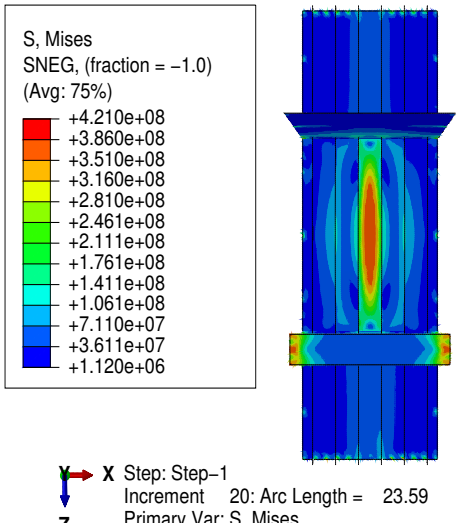

(a) Model 4: von Mises stress for load according to ISO 19906

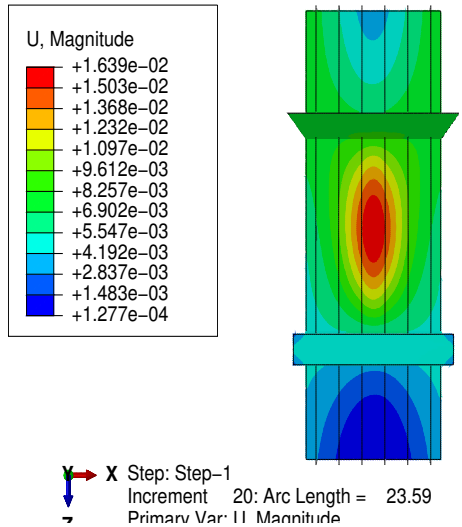

(b) Model 4: Displacement for load according to ISO 19906

Figure A.21

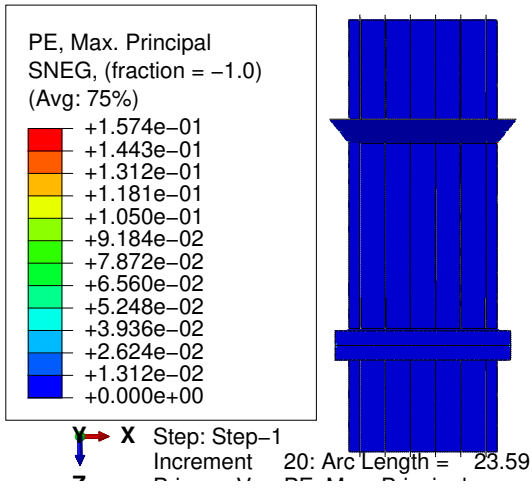

Figure A.22: Model 4: Plastic strain for load according to ISO 19906